

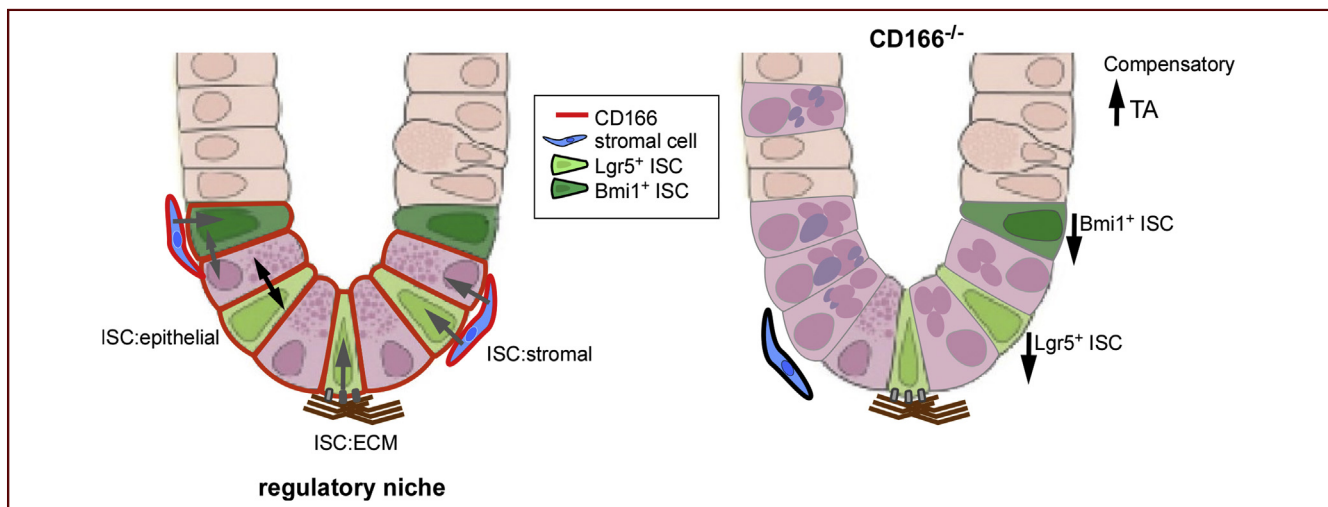
## ORIGINAL RESEARCH

## Cell Adhesion Molecule CD166/ALCAM Functions Within the Crypt to Orchestrate Murine Intestinal Stem Cell Homeostasis



Nicholas R. Smith,<sup>1</sup> Paige S. Davies,<sup>1</sup> Trevor G. Levin,<sup>2</sup> Alexandra C. Gallagher,<sup>1</sup> Douglas R. Keene,<sup>3</sup> Sidharth K. Sengupta,<sup>1</sup> Nikki Wieghard,<sup>4</sup> Edward El Rassi,<sup>5</sup> and Melissa H. Wong<sup>1,6</sup>

<sup>1</sup>Department of Cell, Developmental and Cancer Biology and Oregon Health & Science University, Portland, OR 97239, USA; <sup>2</sup>Department of Biomedical Engineering, Oregon Health & Science University, Portland, Oregon; <sup>3</sup>Shriners' Hospital for Children, Portland, Oregon; <sup>4</sup>Department of Surgery and <sup>5</sup>Department of Otolaryngology, Oregon Health & Science University, Portland, Oregon; and <sup>6</sup>OHSU Stem Cell Center, Knight Cancer Institute, Oregon Health & Science University, Portland, Oregon



## SUMMARY

The cell adhesion molecule and intestinal epithelial crypt-based marker, CD166, functions to maintain the homeostatic niche. Loss of CD166 resulted in decreased active-cycling ISCs and blocked Paneth cell differentiation through a Wnt-deficient signaling environment, highlighting the importance of stem-niche cell interaction in tissue homeostasis.

**BACKGROUND & AIMS:** Intestinal epithelial homeostasis is maintained by active-cycling and slow-cycling stem cells confined within an instructive crypt-based niche. Exquisite regulating of these stem cell populations along the proliferation-to-differentiation axis maintains a homeostatic balance to prevent hyperproliferation and cancer. Although recent studies focus on how secreted ligands from mesenchymal and epithelial populations regulate intestinal stem cells (ISCs), it remains unclear what role cell adhesion plays in shaping the regulatory niche. Previously we have shown that the cell adhesion molecule and cancer stem cell marker, CD166/ALCAM (activated leukocyte cell adhesion molecule), is highly expressed by both active-cycling Lgr5<sup>+</sup> ISCs and

adjacent Paneth cells within the crypt base, supporting the hypothesis that CD166 functions to mediate ISC maintenance and signal coordination.

**METHODS:** Here we tested this hypothesis by analyzing a CD166<sup>-/-</sup> mouse combined with immunohistochemical, flow cytometry, gene expression, and enteroid culture.

**RESULTS:** We found that animals lacking CD166 expression harbored fewer active-cycling Lgr5<sup>+</sup> ISCs. Homeostasis was maintained by expansion of the transit-amplifying compartment and not by slow-cycling Bmi1<sup>+</sup> ISC stimulation. Loss of active-cycling ISCs was coupled with deregulated Paneth cell homeostasis, manifested as increased numbers of immature Paneth progenitors due to decreased terminal differentiation, linked to defective Wnt signaling. CD166<sup>-/-</sup> Paneth cells expressed reduced Wnt3 ligand expression and depleted nuclear  $\beta$ -catenin.

**CONCLUSIONS:** These data support a function for CD166 as an important cell adhesion molecule that shapes the signaling microenvironment by mediating ISC-niche cell interactions. Furthermore, loss of CD166 expression results in decreased ISC and Paneth cell homeostasis and an altered Wnt microenvironment. (*Cell Mol Gastroenterol Hepatol* 2017;3:389–409; <http://dx.doi.org/10.1016/j.jcmgh.2016.12.010>)

**Keywords:** Intestinal Stem Cell; Homeostasis; Paneth Cell; CD166; Stem Cell Niche.

See editorial on page 297.

The continuous renewal and dynamic repair of the intestinal epithelium are fueled by functionally distinct populations of intestinal stem cells (ISCs) located in a confined and instructive microenvironment, the stem cell niche, at the crypt base. Within the niche, cues from adjacent epithelium<sup>1</sup> or underlying stromal cells<sup>2,3</sup> differentially govern these diverse stem and progenitor cells, instructing them to remain quiescent, proliferate, differentiate, or to activate a rapid response to epithelial injury—all to maintain epithelial homeostasis. Within the crypt, ISCs expressing the Wnt target gene *Lgr5*,<sup>4</sup> defined to be active-cycling,<sup>4–6</sup> are located in close proximity to ISCs that are described to be slow-cycling or quiescent<sup>7</sup> (eg, *Bmi1*,<sup>8</sup> *mTert*<sup>9</sup>). The complex cellular relationships between these different classifications of stem cell populations are only beginning to be elucidated in various contexts—homeostasis, after injury, and in disease. Slow-cycling cells, expressing *Bmi1*, have been shown to give rise to the active-cycling ISC pool.<sup>10,11</sup> Adding to this complexity are the recent findings that injury induces committed progenitors to reacquire stemness and contribute to reestablishing the active-cycling stem cell pool.<sup>12–14</sup> Hence, there are multiple ways to maintain and regenerate the active-cycling stem cell domain,<sup>15</sup> highlighting the need for coordinated proliferative regulation of these cells to establish or reestablish homeostasis. Despite an intense focus on ISC dynamics during the past 10 years,<sup>7,8,11,16</sup> an understanding of how distinct stem cell populations are differentially and coordinately regulated is not clear. Although there are studies describing stem cells as harboring intrinsic regulatory programs,<sup>17</sup> it is suggested that the dominant influence derives from the niche.<sup>18,19</sup>


The ISC niche is composed of both crypt epithelium and surrounding stromal cells.<sup>20,21</sup> The active-cycling *Lgr5*<sup>+</sup> ISCs are interspersed between differentiated Paneth cells that provide additional regulatory factors, including a multitude of Wnt ligands<sup>1,22</sup> to drive both *Lgr5*<sup>+</sup> ISC proliferation and Paneth cell differentiation.<sup>23</sup> Physiologic redundancy within the niche exists, exemplified by studies ablating *Wnt3* production from Paneth cells.<sup>2</sup> Loss of this important epithelial-derived signal did not result in loss of the Wnt-dependent *Lgr5*<sup>+</sup> ISC population due to redundant Wnt ligand supply from cells within the crypt-based stroma.<sup>2,3,24</sup> With the influence of both epithelial and stromal factors on proliferation and differentiation within tight quarters, it is likely that an active process exists to differentially regulate the proliferative and quiescence status of ISC populations.

Distinct expression of cell adhesion molecules on cells within the stem cell niche has been reported in numerous organ systems.<sup>25,26</sup> We have previously identified a tightly restricted, high expression domain of the cell adhesion molecule CD166/ALCAM (activated leukocyte cell adhesion molecule) on crypt-based epithelial cells within the niche of

the small intestine and colon.<sup>26</sup> Interestingly, CD166 is expressed on both active-cycling *Lgr5*<sup>+</sup> ISCs as well as their Wnt ligand-producing Paneth cell neighbors (Figure 1A). This restricted expression domain strongly supports that CD166 plays an important regulatory function in ISC maintenance and proliferative capacity. It is well-accepted that cell adhesion molecules function to bring cells together in physical proximity and impact their shape and polarity.<sup>27</sup> In addition, it is possible that they function to direct the myriad of signals from within the niche to influence ISCs.<sup>27</sup> Notably, adherens junctions represent a critical node of cell-cell contact through coordination of a number of cell signaling networks. Robust evidence exists that many adherens junctional proteins, including the E-cadherin-associated protein  $\beta$ -catenin, can localize to the nucleus and participate in key developmental signaling processes.<sup>28</sup>

CD166 is a transmembrane adhesion protein belonging to the immunoglobulin-like domain superfamily.<sup>29,30</sup> In other organ systems CD166 has a reported myriad of functions. This conserved cell adhesion protein participates in physiologic processes including leukocyte intravasation across the blood-brain barrier, monocyte migration across endothelial junctions, angiogenesis, capillary formation, protection against apoptosis in breast cancer cells, and T-cell activation by both antigen-presenting and tumor cells.<sup>31–37</sup> Furthermore, CD166 has been described as a ligand that functions in heterotypic interactions, binding CD6 on T cells,<sup>38–40</sup> acting in homophilic adhesion complexes between epithelial cells,<sup>41</sup> and as a cell surface marker for a subset of hematopoietic progenitor cells,<sup>42,43</sup> multipotent mesenchymal stem cells,<sup>44,45</sup> and cancer stem cells.<sup>46</sup> Recently, CD166 was reported to be expressed on both hematopoietic stem cells and supportive osteoblasts and to be important in maintaining functional stem cell niche interactions within the bone marrow.<sup>47</sup> Whether this maintenance-associated function is due to the regulation of signaling cues to the stem cell is unclear. Although CD166 currently does not have a defined role in regulating specific cell signaling pathways, it is known that CD166 is a direct target of *Wnt5A*, a ligand of the non-canonical Wnt signaling pathway.<sup>48</sup> The non-canonical and canonical Wnt signaling pathways function in a regulatory feedback loop to modulate the reciprocal pathway. This intimate relationship between *Wnt5A* and the canonical Wnt signaling pathway has been demonstrated in many dysregulated and diseased states.<sup>49</sup>

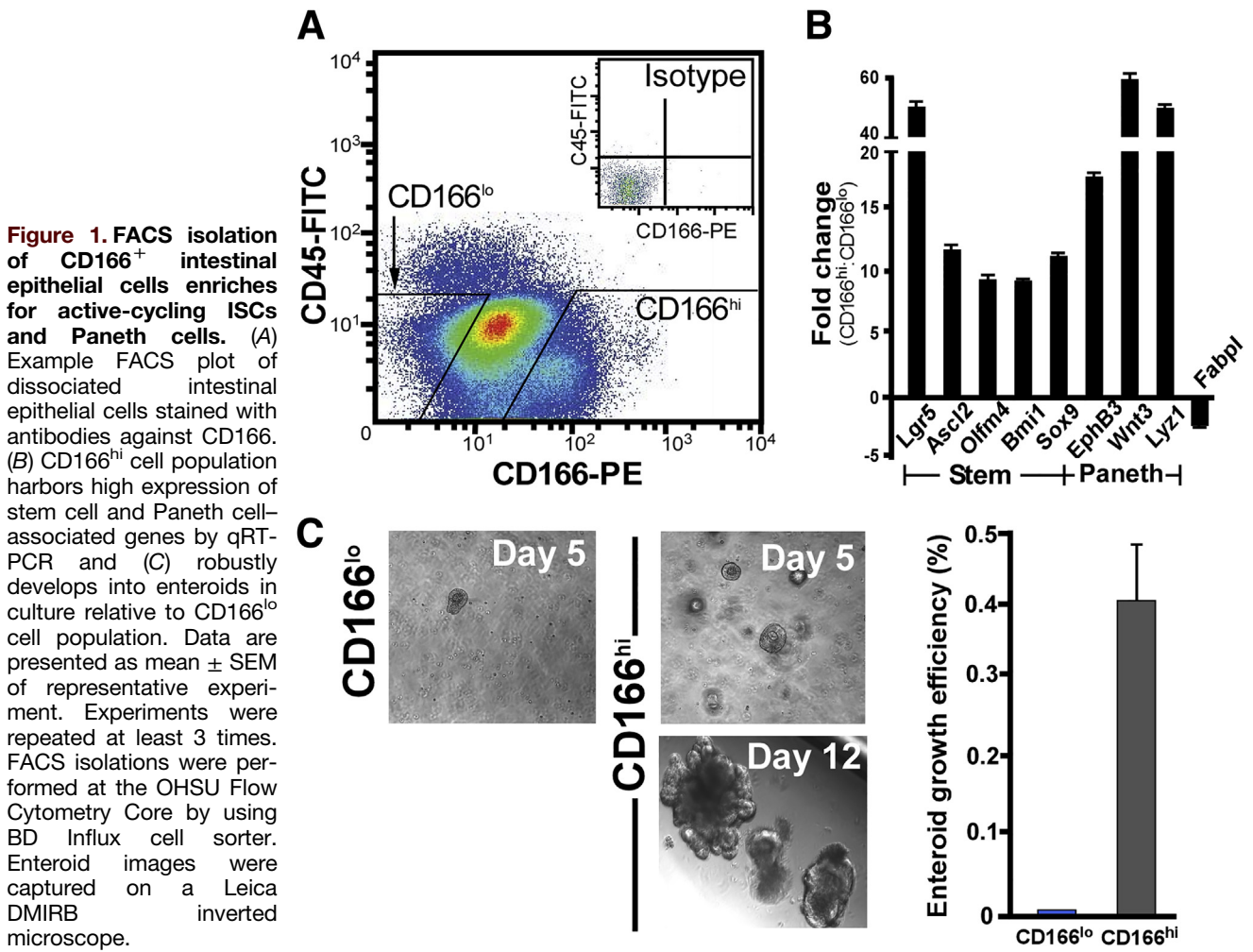
**Abbreviations used in this paper:** BrdU, bromodeoxyuridine; CLEM, correlative light and electron microscopy; FACS, fluorescence-activated cell sorting; FITC, fluorescein isothiocyanate; GFP, green fluorescent protein; HBSS, Hank's balanced salt solution; IHC, immunohistochemistry; ISC, intestinal stem cell; Lyz, lysozyme; Muc2, mucin 2; qRT-PCR, quantitative reverse transcription polymerase chain reaction; SEM, standard error of the mean; TA, trans-activating; TEM, transmission electron microscopy; WT, wild-type.

 Most current article

© 2017 The Authors. Published by Elsevier Inc. on behalf of the AGA Institute. This is an open access article under the CC BY-NC-ND license (<http://creativecommons.org/licenses/by-nc-nd/4.0/>).

2352-345X

<http://dx.doi.org/10.1016/j.jcmgh.2016.12.010>



Although expression of cell adhesion molecules has been reported on various stem cell populations, their discrete physiologic function in this context has not been clearly defined.<sup>27</sup> It is possible that they function to retain the stem cell within a specific regulatory microenvironment, or they may function within junctional complexes to impart differential signaling influences that direct proliferation or differentiation. To test the hypothesis that the stem cell niche adhesion molecule CD166 mediates ISC homeostasis, we systematically explored the functional impact of CD166 loss on the active-cycling ISC domain in CD166<sup>-/-</sup> mice. By using combined approaches of immunohistochemistry (IHC) and fluorescence-activated cell sorting (FACS) analyses, along with molecular and genetic studies, we reveal important functions for CD166 in shaping cell-cell communication within the crypt. Our data support that CD166 functions to maintain active-cycling ISC homeostasis and in directing terminal lineage differentiation of the Paneth cell, mechanistically through mediation of cell-cell interactions that support reception of Wnt and Notch signals. Furthermore, we demonstrate that CD166 is only expressed on a subset of slow-cycling Bmi1<sup>+</sup> ISCs. Bmi1<sup>+</sup> ISCs have demonstrated

capacity to expand and replenish the active-cycling stem cell population after injury,<sup>10,15</sup> indicating that CD166 expression may also function as a mediator of active proliferation.

## Materials and Methods

### Mice

All mouse experiments were performed in accordance to the guidelines issued by the Animal Care and Use Committee at Oregon Health & Science University. Mice were housed in a specific pathogen-free environment under strictly controlled light cycle conditions, fed a standard rodent lab chow (#5001 PMI Nutrition International; Purina Mills LLC, Richmond, IN), and provided water ad libitum. The following strains were used in the described studies: C57BL/6J (JAX #000664), B6.129P2-Lgr5<sup>tm1(cre/ERT2)Cle</sup>/J (Lgr5-GFP; JAX #008875),<sup>16</sup> B6.Cg-Ptprc<sup>b</sup>Bmi1<sup>tm1llwThy1<sup>a</sup></sup>/J (Bmi1-GFP; JAX #017351),<sup>50</sup> B6.129(FVB)-Alcam<sup>tm1Jaww</sup>/J, CD166<sup>-/-</sup> (JAX #010635)<sup>51</sup> mice. All mice were initially obtained from the Jackson Laboratory and were 8–10 weeks of age. A range of n = 3–12 mice were used in each experiment, with biologic and experimental replicates

conducted. When possible, controls were littermates housed in the same cage as experimental animals.

### Image Scoring, Quantification, and Statistics

Described studies used a range of  $n = 3-12$  total mice per genotype. For tissue staining analysis,  $n = 4-8$  mice were analyzed and 25–100 crypts scored per animal, except where noted. For flow cytometry/FACS, Western blotting, quantitative reverse transcription polymerase chain reaction (qRT-PCR), and enteroid growth analyses,  $n = 3-12$  mice were used per study in at least 3 technical experimental repeats. Unless otherwise noted, statistical significance was determined by an unpaired Student's  $t$  test with Welch's correction. All statistical analyses were performed by using GraphPad Prism software (LaJolla, CA). A value of  $P < .05$  was determined as statistically significant. Data are presented as the mean  $\pm$  standard error of the mean (SEM).

### Tissue Preparation, Staining, and Microscopy

Mouse intestines were processed as we have previously described.<sup>26,52</sup> Briefly, proximal or distal small intestine was fixed in 4% paraformaldehyde for 1 hour at room temperature and then processed for paraffin or frozen tissue analyses. Histochemical or IHC analyses were performed on 5  $\mu\text{m}$  tissue sections, and hematoxylin-eosin, alcian blue/nuclear fast red, or antibody staining was conducted as we have previously reported.<sup>26,52</sup> Morphometric analysis of crypt depth was performed on hematoxylin-eosin-stained

tissues that were digitally imaged on the Aperio automated slide scanner (Leica, Wetzlar, Germany), and crypt depth was measured by using ImageScope software (Leica). Only well-oriented crypts with a visible lumen and continuous, uniform epithelial layer from crypt base through the villus junction were scored. To measure crypt cell proliferation, mice were intraperitoneally injected with 120  $\mu\text{g/g}$  5-bromo-2-deoxyuridine (BrdU) (Sigma-Aldrich, St Louis, MO) 2 hours before death. For immunofluorescence, primary antibodies listed in Table 1 were used, followed by detection with appropriate species-specific fluorescent secondary antibodies (Alexa-488, 1:500, Molecular Probes, Eugene, OR; Cy3 and Cy5, 1:500, Jackson Immuno Research, West Grove, PA) and imaged by using a Leica DMR upright fluorescent microscope or Olympus (Tokyo, Japan) BX61 confocal microscope controlled by FluoView software (Olympus America, Center Valley, PA). For confocal images, 1- $\mu\text{m}$ -thick optical sections were captured spanning the entire tissue thickness. IHC staining was performed by using the ABC kit (Vector Labs, Burlingame, CA) according to the manufacturer's instructions. Paraffin or frozen tissue was processed and analyzed for IHC/immunofluorescence as we have previously reported.<sup>26,52</sup>

### Intestinal Crypt Isolation and Assays

Mouse small intestines were isolated as we have previously published,<sup>53</sup> with the following exceptions. After tissue shaking, crypts were enriched by filtration through

**Table 1.** Antibodies Used in the Present Study

Antigen	Company	Catalog no.	Dilution	Antigen retrieval
<b>Antibodies for IHC/immunofluorescence</b>				
CD166	R&D Systems	AF1172	500	N/A
GFP	Life Technologies	A11122	500	N/A
GFP	Aves	GFP-1020	1000	N/A
Lysozyme	DAKO	A0099	500	N/A
Lysozyme	The Binding Site	PC073	200	N/A
E-cadherin	Sigma	U3254	500	N/A
E-cadherin	Cell Signaling	3195	200	N/A
ZO-1	Chemicon	MAB1520	50	N/A
BrdU	Gift from J. Gordon	N/A	1000	Sodium citrate pH 6
Ki67	Abcam	ab15580	1000	N/A
PHH3	Cell Signaling	9701	200	Sodium citrate pH 6
Muc2	Santa Cruz	sc-15334	200	N/A
$\beta$ -catenin	BD Transduction Labs	610154	100	Sodium citrate pH 6
ChgrA	Abcam	ab15160	500	N/A
Notch-ICD	Cell Signaling	4147	100	Sodium citrate pH 6
<b>Antibodies for Flow/FACS</b>				
CD166-PE	R&D Systems	FAB1172P	200	
CD45-FITC	eBioscience	11-0454-85	200	
CD31-PE-Cy7	Biolegend	102418	200	
CD45-PE-Cy7	Biolegend	103114	200	
mAb B6A6	MWong lab	N/A	Undiluted	
Anti-rat IgG-PE	Jackson	712-116-153	200	
Anti-rat IgG-APC	Jackson	712-136-153	200	
<b>Antibodies for Western blotting</b>				
ZO-1	Chemicon	MAB1520	500	
E-cadherin	Sigma	U3254	1000	
Notch-ICD	Cell Signaling	4147	1000	
Tubulin (B512)	Sigma	T5168	5000	
Tubulin	Sigma	SAB4500087	5000	



100  $\mu\text{m}$  and 70  $\mu\text{m}$  cell strainers (BD Biosciences, Franklin Lakes, NJ) and subsequently prepared for enteroid culture, flow cytometry/FACS, or protein lysate.

***In vitro growth.*** Enteroids were established from freshly isolated proximal small intestinal crypts according to standard protocols.<sup>54</sup> Crypts were seeded in 50  $\mu\text{L}$  growth factor reduced Matrigel (Corning Life Sciences, Corning, NY) drops at 1000 crypts/mL into pre-warmed 24-well tissue culture plates and then overlaid with enteroid culture media (Advanced DMEM/F12 + 10 mmol/L HEPES, 4 mmol/L L-glutamine, 1 $\times$  N2 supplement and B27 supplements [and 1 $\times$  penicillin/streptomycin], all from Gibco Laboratories, Gaithersburg, MD), and the following growth factors: Jagged-1 peptide (1  $\mu\text{mol/L}$ ; Anaspec, Fremont, CA), Egf (50 ng/mL; R&D Systems, Minneapolis, MN), Noggin (100 ng/mL; Peprotech, Rocky Hill, NJ), and Rspo1 (1  $\mu\text{g/mL}$ ; R&D Systems). Enteroids were imaged by using either a Leica DMIRB or Nikon Eclipse TE200 inverted microscope. Live imaging was performed by using an Incucyte ZOOM microscope system (Essen BioScience Inc, Ann Arbor, MI). Enteroid growth and budding were quantified from images by using ImageJ (National Institutes of Health, Bethesda, MD).

***Flow cytometry analysis and fluorescence-activated cell sorting.*** By using our previously published methods,<sup>53,55</sup> intestinal crypts were centrifuged at 4°C at 1000 rpm for 5 minutes and subsequently dissociated to single cells by incubation in 10 mL Hank's balanced salt solution (HBSS) + 0.3 U/mL Dispase (Gibco), 50  $\mu\text{g/mL}$  DNase I (Roche Diagnostics, Indianapolis, IN), and 10  $\mu\text{mol/L}$  Y-27632 (Stemgent, Cambridge, MA) at 37°C for 10 minutes with vigorous shaking every 2–3 minutes. Single cells were filtered through a 40- $\mu\text{m}$  cell strainer and then stained with antibodies listed in Table 1. Single cells were sorted to purity on a BD Influx FACS machine at the Oregon Health and Science University flow cytometry shared resource. For qRT-PCR analysis of crypt-based epithelial cell gene expression, dissociated intestinal epithelial cells were stained with antibodies to CD31, CD45, and rat monoclonal antibody B6A6.<sup>55</sup> qRT-PCR was conducted on the live B6A6<sup>+</sup>, CD31/45<sup>+</sup> cell population. For single cell enteroid culture, FACS-isolated cells were seeded in Matrigel (200 cells/ $\mu\text{L}$ ) and cultured as described above. Enteroid growth efficiency was determined as the number of enteroids after 10 days in culture per the number of cells seeded in each Matrigel drop. For proliferation analysis of Bmi1-GFP<sup>+</sup> cell populations, Bmi1-GFP<sup>+</sup>/CD166<sup>lo</sup> and Bmi1-GFP<sup>+</sup>/CD166<sup>hi</sup> populations were isolated onto slides and stained for Ki67. The percentage of Ki67<sup>+</sup> nuclei per total nuclei observed is reported. FACS plots and data analyses were performed using FlowJo (Tree Star, Ashland, OR).

***Immunoblot analyses of intestinal crypt lysates.*** Isolated crypts were pelleted and resuspended in ice cold 1 $\times$  RIPA buffer (50 mmol/L Tris pH7.5, 150 mmol/L NaCl, 1 mmol/L ethylenediamine tetraacetic acid, 1% NP-40, 0.5% deoxycholic acid, 0.1% sodium dodecylsulfate) supplemented with protease inhibitor cocktail (Roche) and phosphatase inhibitors 5 mmol/L sodium fluoride and 2 mmol/L sodium orthovanadate (Sigma-Aldrich), followed by lysis

with a 23-gauge needle. Cellular debris was pelleted, and supernatants were mixed with Laemmli sample buffer and denatured by boiling for 5 minutes. Total protein (20  $\mu\text{g}$ ) was separated by sodium dodecylsulfate polyacrylamide gel electrophoresis and transferred to nitrocellulose membranes. Membranes were blocked with 1 $\times$  TBS + 5% bovine serum albumin for 1 hour at 20°C and then probed with the primary antibodies listed in Table 1. After washing and incubation with the appropriate IRDye coupled secondary antibodies, blots were imaged on a LiCor Biosciences (Lincoln, NE) Odyssey scanner, and densitometry was analyzed relative to the tubulin loading control by using ImageJ software. Total protein concentration of crypt lysates was determined by BCA assay (Thermo Fisher Scientific, Agawam, MA).

### ***Mesenchyme Isolation for Quantitative Reverse Transcription Polymerase Chain Reaction Analysis***

After intestinal epithelial cells were dissociated by shaking as described above, remnant tissues were further washed in ice cold HBSS. Mesenchymal cells were then isolated by scraping remnant tissues with a glass coverslip into ice cold HBSS. Scraped mesenchymal cells were subsequently filtered through a 40  $\mu\text{mol/L}$  cell strainer (BD Biosciences), pelleted by centrifugation at 4°C at 1000 rpm for 5 minutes, and then lysed into RNAqueous lysis buffer (Ambion, Austin, TX) for subsequent RNA extraction and cDNA synthesis.

### ***RNA Extraction and Quantitative Reverse Transcription Polymerase Chain Reaction***

RNA was extracted by using the RNAqueous Micro Kit (Ambion) according to the manufacturer's protocols. RNA quality was determined with an Agilent 2100 BioAnalyzer, followed by complementary DNA synthesis using the high capacity complementary DNA synthesis kit (Applied Biosystems). qRT-PCR was performed by using a SYBR Green-based assay and ViiA 7 real-time PCR system (Applied Biosystems) according to established protocols.<sup>26</sup> Each complementary DNA sample was analyzed in triplicate, along with triplicate samples of the endogenous reference gene, glyceraldehyde-3-phosphate dehydrogenase, in a minimum of  $n = 3$  technical and biologic replicates. Primers used are listed in Table 2.

### ***Intestinal Barrier Integrity Assay***

Mice were fasted for 3 hours before gavage with fluorescein isothiocyanate (FITC)-dextran (0.5 mg/g; Sigma-Aldrich). Four hours after gavage, mice were killed, and 150  $\mu\text{L}$  whole blood was isolated into 100  $\mu\text{L}$  HBSS + 50 U/mL heparin. Red blood cells were pelleted by centrifugation at 1000 rpm for 5 minutes. Raw FITC fluorescence from the resulting blood serum was measured on a Glomax fluorimeter (Promega, Madison, WI). All fluorescence intensities were normalized to phosphate-buffered saline-gavaged control serum. For cytokine-injected controls, wild-type

(WT) mice were injected with a mixture of recombinant tumor necrosis factor- $\alpha$ /interferon- $\gamma$  (500 ng each; Peprrotech) 24 hours before gavage.<sup>56</sup>

### Correlative Light and Electron Microscopy

Intestines were isolated as we previously described,<sup>57</sup> and the luminal contents were flushed with ice cold 1 $\times$  PIPES, HEPES, EGTA, and MgCl<sub>2</sub> buffer pH 6.9.<sup>58</sup> Cross sections approximately 2 mm in thickness were immersed in 1 $\times$  PIPES, HEPES, EGTA, and MgCl<sub>2</sub> buffer + 4% para-formaldehyde, 0.05% glutaraldehyde for 1 hour at 20°C, followed by incubation at 4°C overnight. The tissues were washed in 100 mmol/L Tris pH 7.4, dehydrated in 90% ethanol, and then infiltrated and embedded in LR-White resin (Ted Pella Inc, Redding, CA) according to standard protocols.<sup>59</sup> Ultrathin 90 nm sections were cut by using a Leica UC7 ultramicrotome and mounted onto Formvar-coated single-hole nickel slot grids. Grids were floated (section

side down) on 150 mmol/L Tris pH 7.4 + 50 mmol/L glycine, followed by incubation with blocking buffer (Tris pH 7.4 + 2% non-fat dry milk, 0.5% ovalbumin, and 0.5% fish gelatin) for 30 minutes at 20°C and then incubated with primary antibody (rabbit anti-lysozyme, 1:50; Dako, Carpinteria, CA) for 2.5 hours at 20°C. After washing, grids were incubated with Alexa-488, 10 nm gold dually conjugated secondary antibody (1:10; Life Technologies, Carlsbad, CA) for 1 hour at 20°C, washed in distilled water, and dried before imaging by using the FEI Tecnai with iCorr (Fei Company, Hillsboro, OR) integrated fluorescence and transmission electron microscopy (TEM) microscope at the Oregon Health and Science University Multi-scale Microscopy Core. No contrasting agents were used on the ultrathin tissue sections. A total of  $n = 5$  mice/genotype were processed, and  $n = 6-8$  crypts/animal were imaged.

## Results

### CD166 Expression Delineates the Active-cycling Intestinal Stem Cell Domain

Our earlier studies revealed an intriguing expression pattern for the cell adhesion molecule CD166, with high levels within the base of small and large intestinal crypts.<sup>26</sup> Therefore, to determine whether CD166 functions in homeostatic control within the ISC domain, we first verified specific CD166 expression on discrete stem cell populations. Robust cell surface expression of CD166 facilitated isolation and characterization of cells by FACS<sup>55</sup> (Figure 1A). CD166<sup>hi</sup> epithelial cells harbored enriched expression of stem cell marker genes including both the active-cycling Lgr5<sup>+</sup> and slow-cycling Bmi1<sup>+</sup> populations (Figure 1B), although there was notably greater enrichment in Lgr5 expression. In addition, these cells were strongly enriched in Paneth cell marker genes (Figure 1B). As expected from a population harboring both active-cycling Lgr5<sup>+</sup> ISCs and Paneth cells, CD166<sup>hi</sup> crypt-based cells initiated intestinal enteroid growth more efficiently than the CD166<sup>lo</sup> population (Figure 1C) under standard published culture conditions.<sup>54,55</sup> These data revealed that high CD166 expression demarcates the active-cycling ISC domain.

To further evaluate CD166 expression within the ISC zone, intestinal epithelial cells expressing green fluorescent protein (GFP) under control of ISC promoters, either active-cycling (Lgr5<sup>16</sup>) or slow-cycling (Bmi1<sup>50</sup>), were analyzed by immunofluorescence and flow cytometry (Figure 2). Consistent with our previous work,<sup>26</sup> the CD166 expression domain encompassed both differentiated secretory Paneth cells and the juxtaposed active-cycling ISC population expressing the Wnt target gene Lgr5<sup>16</sup> (Figure 2A). Interestingly, the majority of a slow-cycling stem cell population expressing Bmi1<sup>50</sup> resided outside of the CD166 expression domain (Figure 2C, white arrowhead), although a subset of CD166-expressing Bmi1<sup>+</sup> ISCs were localized to the crypt base, 19.6% (Figure 2D, yellow arrowhead). This was confirmed by flow cytometry (Figure 2E) and was in contrast to the Lgr5<sup>+</sup> ISC population where the majority of cells, 92%, expressed CD166 (Figure 2B). Cellular localization of CD166 protein on both Lgr5<sup>+</sup> and Bmi1<sup>+</sup> ISC

**Table 2.** qRT-PCR Primers Used in the Present Study

Target	F/R	Sequence (5'-3')
<i>Ascl2</i>	F	CCGGTTCCTCGCGAGCACTTTT
	R	TCCAGACGAGGTGGGCATGAGT
<i>Bmi1</i>	F	TATACTGATGATGAGATAATAAGC
	R	CTGGAAAGTATTGGGTATGTC
<i>Defcrl1</i>	F	AGCAGCCATTGTGCGAAGAA
	R	TGCTGTGATTTGGAGCTTGG
<i>Egf</i>	F	CCTCGCCCGGACTGAGTTGC
	R	GCACACGCCACCATTGAGGCA
<i>Dll1</i>	F	GGACGATGTTCCAGATAACCC
	R	CCACATTGTCTCGCAGTA
<i>EphB3</i>	F	AAGAGACTCTCATGGACACGAAT
	R	ACTTCCC GCCGCCAGATG
<i>Fabpl</i>	F	GGTCTGCCCGAGGACCTCAT
	R	CCAGTTCCGACTCCTCCCCC
<i>Gapdh</i>	F	AAATATGACAACACTCAAGATTGTCA
	R	CCCTTCCACAATGCCAAAGT
<i>Hopx</i>	F	TTCAACAAGGTCAACAAGCACCCG
	R	CCAGGCGCTGCTTAAACCATTCT
<i>Lgr5</i>	F	TTTGAGAAGCCTTCAATCCC
	R	GACAGGGACGTCTGTGAGAG
<i>Lyz1</i>	F	GAGACCGAAGCACCCGACTATG
	R	CGGTTTTGACATTGTGTTTCGC
<i>Mmp7</i>	F	ATGGCAGCTATGCAGCTCACCC
	R	CCATATAACTTCTGAATGCCTGC
<i>mTert</i>	F	GCAGGTGAACAGCCTCCAGACAG
	R	TCCTAACACGCTGGTCAAAGGGAAGC
<i>Olfm4</i>	F	GCCACTTTCCAATTTTCCAC
	R	GAGCCTCTTCTCATAAC
<i>Sox9</i>	F	TGCCCATGCCCGTGCGCGTCAA
	R	CGCTCCGCCTCCTCCACGAAGGGTCT
<i>Wnt2b</i>	F	CACCCGGACTGATCTTGTCT
	R	TGTTTCTGCACTCCTTGAC
<i>Wnt3</i>	F	CAAGCACAACAATGAAGCAGGC
	R	TCGGGACTCACGGTGTCTCTC
<i>Wnt5a</i>	F	CGCTAGAGAAAGGGAACGAATC
	R	TTACAGGCTACATCTGCCAGGTT

F, forward; R, reverse.

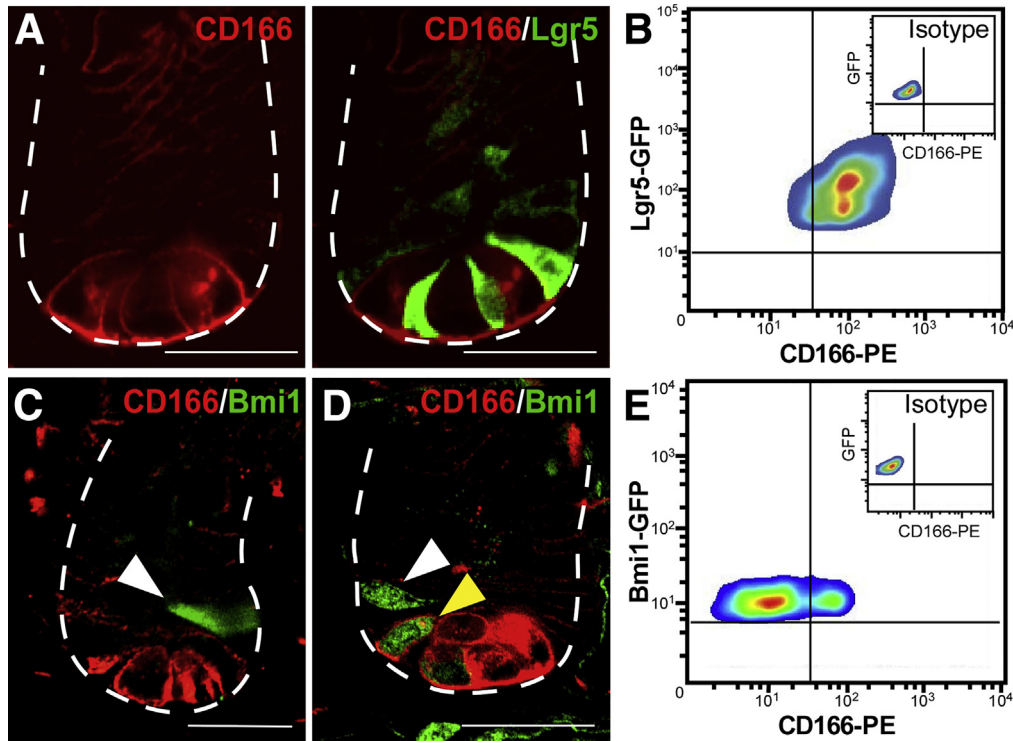


**Figure 2. CD166 expression within the crypt.** (A) Lgr5-GFP reporter mouse intestinal crypt stained with antibodies to CD166 (red). Active-cycling Lgr5-GFP ISCs (green) reside within the CD166-expression domain. (B) Flow cytometry of dissociated intestinal epithelial cells from Lgr5-GFP mice indicate that the majority of Lgr5-GFP<sup>+</sup> cells express CD166. (C and D) Bmi1-GFP reporter mouse intestinal crypt stained for CD166 (red). Majority of slow-cycling Bmi1<sup>+</sup> ISCs (green, white arrowhead) do not express CD166, with a subset that is CD166-expressing (D, yellow arrowhead). White dashed line represents the epithelial-mesenchymal boundary. Scale bars = 25  $\mu$ m. (E) A subset of Bmi1-GFP<sup>+</sup> intestinal epithelial cells expresses CD166 by flow cytometry. Fluorescent images were captured on Olympus BX61 confocal microscope. FACS experiments were performed by using BD Influx cell sorter at OHSU Flow Cytometry Core. Data are representative of experiments repeated at least 3 times.

populations, as well as the differentiated Paneth cell, was distributed to cell-cell junctions and the basolateral surface (Figure 2A, C, and D). Significantly, the differential pattern of expression on the active-cycling relative to the slow-cycling ISC population supports a potential regulatory role for CD166 on active-cycling stem cell behavior. Therefore, we set out to determine whether disrupting the cellular relationship between the Paneth and the active-cycling stem cell directly impacted ISC homeostasis. To explore this possibility, we analyzed the consequence of CD166 loss within the ISC zone by using CD166<sup>-/-</sup> mice. As reported, CD166<sup>-/-</sup> mice were viable and fertile.<sup>51</sup> Importantly, the integrity of the intestinal epithelial barrier was not compromised (Figure 3), despite loss of CD166, which is reported to associate with adherens junctions<sup>60</sup> and is expressed at low levels on the epithelium throughout the crypt-villus unit.<sup>26</sup>

#### Loss of CD166 Perturbs Stem Cell Zone Architecture and Lgr5<sup>+</sup> Intestinal Stem Cell Maintenance

To determine whether loss of CD166 impacted the active-cycling ISC domain, we analyzed the physical structure of the crypt base as well as the stem cell dynamics in intestines of

CD166<sup>-/-</sup> mice on an Lgr5-GFP reporter background.<sup>16</sup> Strikingly, CD166<sup>-/-</sup> intestinal crypts displayed abnormal cellular architecture as depicted by disruption of the normally highly ordered one-to-one Lgr5<sup>+</sup> ISC-to-Paneth cell pattern that is apparent in WT crypts<sup>1</sup> (Figure 4A and B). As reported previously, one school of thought is that maintenance of Lgr5<sup>+</sup> cell stemness and their retention within the crypt are dependent on direct contact with Paneth cells on all sides.<sup>1,61</sup> Indeed, loss of CD166 resulted in a disruption of the Lgr5<sup>+</sup> ISC:Paneth cell ratio (1.0 for WT versus 0.58 for CD166<sup>-/-</sup> crypts) with juxtaposed crypt cell interactions, likely Paneth cells, apparent in both sagittal and cross sections of CD166<sup>-/-</sup> crypts (Figure 4A and B).

Consistent with disruption of the cellular patterning within CD166 null crypts, there was a significant decrease in the number of Lgr5<sup>+</sup> ISCs per crypt (Figure 4C), as determined by quantification of GFP<sup>+</sup> cells in confocal micrographs of whole-mount intestinal tissues. This finding was confirmed by flow cytometry, revealing that CD166<sup>-/-</sup> intestinal crypts contained ~25% fewer Lgr5-GFP<sup>hi</sup> ISCs relative to WT crypts (Figure 4E). Interestingly, reduction of Lgr5<sup>+</sup> ISCs was accompanied by an overall decrease of active-cycling stem cell gene expression within FACS-isolated crypt epithelium but not by slow-cycling or



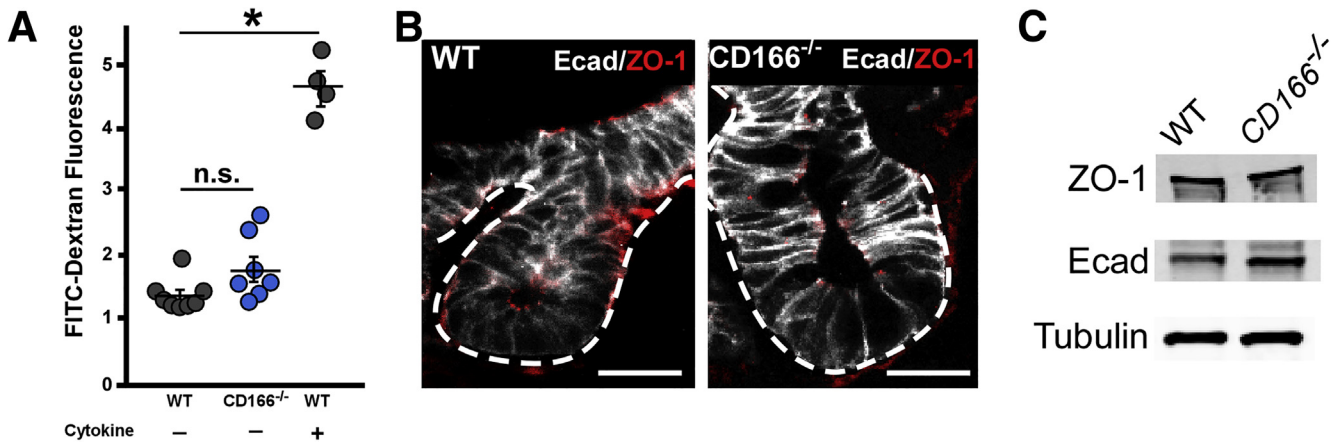


**Figure 3. Loss of CD166 expression does not compromise the intestinal epithelial barrier.** (A) Adult WT ( $n = 9$ ) and CD166<sup>-/-</sup> ( $n = 8$ ) mice gavaged with FITC-dextran were evaluated for presence of fluorescence in peripheral blood. Positive control WT mice ( $n = 4$ ) were injected with cytokines 24 hours before experiment. Data are presented as mean  $\pm$  SEM. \* $P < .05$  by 1-way analysis of variance. (B) Adult WT and CD166<sup>-/-</sup> mouse intestines express comparable E-cadherin (Ecad) and ZO-1 expression as determined by IHC and (C) Western blot analyses. White dashed line represents epithelial-mesenchymal boundary. Scale bars = 25  $\mu$ m. Fluorescent images were captured on Leica DMR upright microscope. Experiments were repeated at least 3 times.

quiescent stem cell gene expression (Figure 4D). Not only were there fewer total Lgr5<sup>+</sup> ISCs in CD166<sup>-/-</sup> crypts, the Lgr5-GFP<sup>hi</sup> ISC population displayed decreased enteroid formation capacity in ex vivo cultures, suggesting reduced stemness of this ISC population (Figure 4F). It has been previously reported that in response to ablation of the Lgr5<sup>+</sup> ISC pool, the slow-cycling Bmi1<sup>+</sup> ISC population is stimulated and expands in a compensatory manner.<sup>10,11</sup> To determine whether the CD166-associated defect was compensated in a similar manner, we analyzed CD166<sup>-/-</sup> crypts on a Bmi1-GFP transgenic reporter background. Unexpectedly, IHC and flow cytometric analyses of this slow-cycling ISC population revealed a decrease in total numbers of Bmi1<sup>+</sup> cells within CD166<sup>-/-</sup> crypts (Figure 5A and B). These data suggest that differential CD166 expression on Bmi1<sup>+</sup> ISCs may alter their ability to proliferate and expand to compensate for the loss of the active-cycling Lgr5<sup>+</sup> ISC population. To determine whether CD166 expression on Bmi1<sup>+</sup> ISCs is associated with a proliferative phenotype, Bmi1<sup>+</sup> ISCs were FACS-isolated from WT crypts, subdivided into CD166<sup>lo</sup> and CD166<sup>hi</sup> populations, and then analyzed for their Ki67<sup>+</sup> proliferative status. Bmi1<sup>+</sup> ISCs harboring high CD166 expression displayed almost 3-fold more Ki67<sup>+</sup> cells than those with low CD166 expression (Figure 5C). Interestingly, FACS-isolated CD166<sup>-/-</sup> Bmi1<sup>+</sup> ISCs retained their spheroid-initiating capacity in culture and displayed equal growth efficiency compared with WT Bmi1<sup>+</sup> ISCs (Figure 5D), suggesting that stimulation within a high Wnt environment rescues the proliferation phenotype.

Despite having fewer Lgr5<sup>+</sup> ISCs, CD166<sup>-/-</sup> crypts contained a greater total cell number (data not shown) and therefore were significantly deeper than WT crypts (Figure 6A). Interestingly, within the Lgr5-GFP<sup>+</sup> cell population, CD166<sup>-/-</sup> intestines had fewer Lgr5-GFP<sup>hi</sup> cells (reported to be stem cells) and more Lgr5-GFP<sup>lo</sup> cells

(reported to represent transit-amplifying [TA] cells fated to differentiate<sup>5,62,63</sup>) compared with controls (Figure 4E). To determine which population was responsible for increased crypt cell numbers, mice were injected with BrdU 2 hours before death. The deeper CD166<sup>-/-</sup> crypts contained more BrdU<sup>+</sup> nuclei relative to WT controls (Figure 6B); however, the majority of proliferating cells were localized to the TA compartment and did not reside within the crypt base (Figure 6B), indicating reduced proliferation from active-cycling ISCs and expansion of the TA zone. These findings were confirmed with analyses of additional antibody markers that recognized different phases of the cell cycle, Ki67 (all phases) and phospho-histone H3 (mitosis) (Figure 6C and D). Taken together, these data indicate that loss of CD166 impedes proliferative status of Lgr5<sup>+</sup> ISCs, may inhibit the compensatory expansion of Bmi1<sup>+</sup> ISCs, and results in a compensatory expansion of the TA compartment.

#### Decreased Stem Cell Fitness in the Active-cycling Zone Is Accompanied by Disruption in Paneth Cell Homeostasis

To determine the underlying cause of disruption in active-cycling ISC dynamics, we examined the status of the Wnt ligand and CD166-expressing Paneth cell, previously demonstrated to provide signaling cues for Lgr5<sup>+</sup> ISC pool maintenance.<sup>1</sup> Histologic analysis of the CD166<sup>-/-</sup> small intestinal epithelium revealed striking differences in morphology and localization of the mature granular eosinophilic Paneth cells normally restricted to the crypt base (Figure 7A, upper panel). In CD166<sup>-/-</sup> crypts, Paneth cells were enlarged, misshapen, and more abundant (Figure 7A, lower panel). In addition, the Paneth cell differentiation marker lysozyme (Lyz) displayed diffuse expression within the crypt base and importantly revealed frequent Lyz<sup>+</sup> cell mislocalization to the upper crypt or villus (Figure 7B



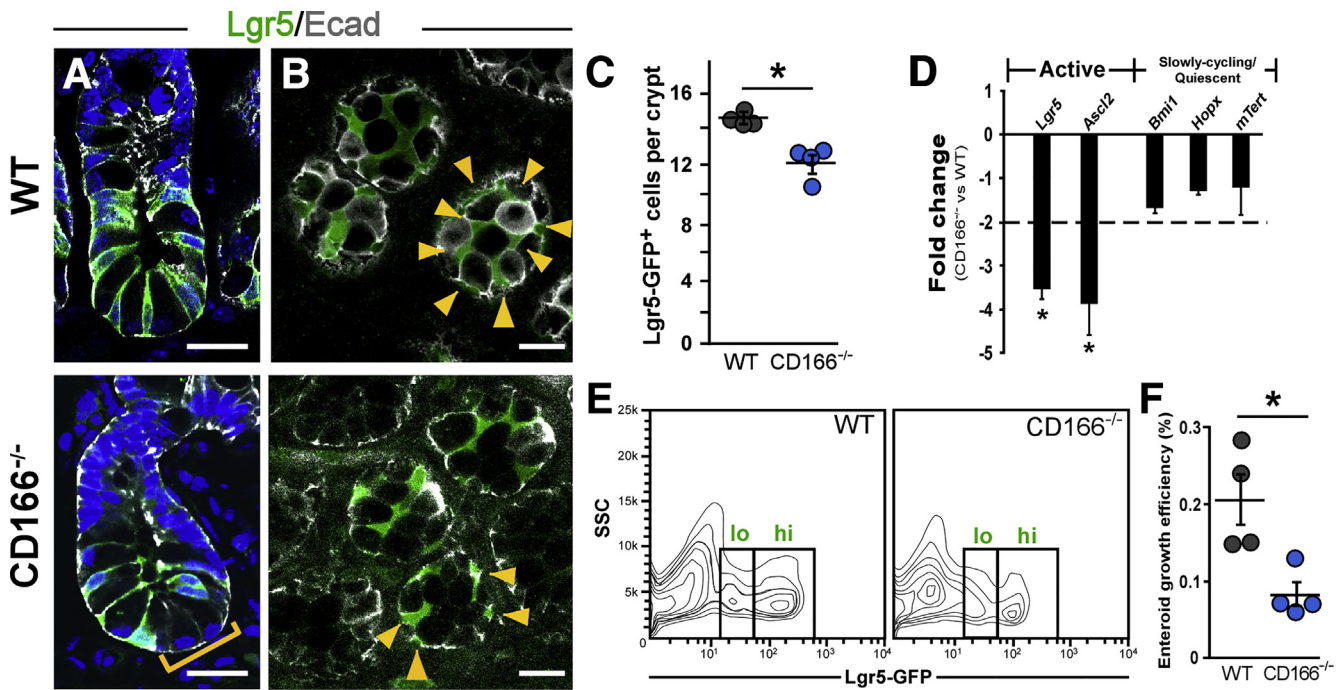


**Figure 4. *Lgr5*<sup>+</sup> stem cell number and function are decreased in *CD166*<sup>-/-</sup> crypts.** Comparison of *Lgr5*<sup>+</sup> ISCs in adult WT (*n* = 4) and *CD166*<sup>-/-</sup> (*n* = 4) mouse intestines. (A) Longitudinal and (B) sagittal sections of intestinal crypt reveal reported interspersed Paneth cell (outlined with E-cadherin, gray) and *Lgr5*<sup>+</sup> stem cell (green, gray) and *Lgr5*<sup>+</sup> stem cell (green, gray) and *Lgr5*<sup>+</sup> stem cell (green, gray) in WT crypts as compared with disorganized pattern in *CD166*<sup>-/-</sup> crypts (lower panels). (C) Quantification of total *Lgr5*-GFP<sup>+</sup> cells per crypt revealed in WT (gray) and *CD166*<sup>-/-</sup> (blue) crypts revealed significant reduction in active-cycling *Lgr5*<sup>+</sup> ISCs in *CD166*<sup>-/-</sup> tissues, *n* = 4 animals per genotype, at least 20 crypts scored per animal. (D) Expression of active and slowly-cycling ISC genes was determined in FACS-isolated crypt-based WT or *CD166*<sup>-/-</sup> intestinal epithelial cells by qRT-PCR. Data are presented as mean ± SEM of at least 3 independent experiments. \**P* < .05 by 1-sample *t* test compared with theoretical mean = -2. (E) FACS analyses of *Lgr5*-GFP<sup>+</sup> cells reveal fewer total *Lgr5*-GFP<sup>+</sup> cells in *CD166*<sup>-/-</sup> intestinal crypts (27% vs 22%) and decreased pool of *Lgr5*-GFP<sup>hi</sup> (stem cells, 56% vs 45%) and relative increase in *Lgr5*-GFP<sup>lo</sup> cells (TA cells, 44% vs 55%) in *CD166*<sup>-/-</sup> intestinal crypts. Study represents data from 4 separate cell sorting experiments *n* = 8–10 mice total for each genotype. (F) FACS-isolated *Lgr5*-GFP<sup>hi</sup> cells from *CD166*<sup>-/-</sup> intestines have reduced enteroid forming capacity compared with WT controls. Data are representative of experiments repeated 3 times. Fluorescent images were captured on Olympus BX61 confocal microscope. FACS experiments were performed by using BD Influx cell sorter at OHSU Flow Cytometry Core. Data are presented as mean ± SEM. \**P* < .05. Scale bars = 25 μm.

and C). Co-staining of the adherens junction protein E-cadherin facilitated quantification of *Lyz*-expressing cells and revealed increased total numbers within *CD166*<sup>-/-</sup> crypt sections. Furthermore, Paneth cell differentiation gene expression, including *Lyz* and *Defensin*, was dramatically reduced in *CD166*<sup>-/-</sup> FACS-isolated crypt epithelium (Figure 7D), indicating that CD166 participates in mediating Paneth cell maturation and homeostasis. Importantly, gene expression of key regulatory factors including *Wnt3* and *Egf*, which are involved in ISC maintenance and proliferation, were also significantly reduced, consistent with an impaired stem cell microenvironment. Notably, examination of the other major secretory lineages, goblet and enteroendocrine cells, revealed that these cell types were also expanded in numbers within *CD166*<sup>-/-</sup> tissues (Figure 8).

The observed increase in *Lyz*<sup>+</sup> cells within *CD166*<sup>-/-</sup> tissues, with concomitant decrease in Paneth cell marker gene expression, could reflect expansion of Paneth cell progenitors and/or a block in terminal differentiation of the Paneth lineage. Therefore, we first asked whether there was increased specification of Paneth cell progenitors in

*CD166*<sup>-/-</sup> intestines. To determine this, we evaluated the presence of bipotential Paneth-goblet secretory progenitor cells within the crypt. These normally rare progenitor cells co-express products for Paneth (ie, *Lyz*) and goblet cells (ie, Mucin2 [*Muc2*])<sup>64,65</sup> and are detected in approximately 5%–10% of crypts during homeostasis, localized to the upper crypt above the active-cycling domain<sup>66</sup> (Figure 7B, white arrow, and Figure 9A). To explore whether CD166 loss impacts the number of bipotential secretory progenitors, thereby increasing Paneth cell specification, a Notch-directed process,<sup>67,68</sup> tissues were double-stained with antibodies to *Lyz* and *Muc2*. As expected for WT intestines, mature Paneth cells residing in the crypt base only expressed *Lyz*, whereas rare *Lyz*<sup>+</sup>/*Muc2*<sup>+</sup> bipotential progenitors were positioned in the upper crypt (Figure 7E, white arrowhead). Conversely, in *CD166*<sup>-/-</sup> intestines, the vast majority of crypt-based *Lyz*<sup>+</sup> cells also co-expressed *Muc2* (Figure 7E), indicating that loss of CD166 resulted in increased specification and an expansion of progenitor-like or immature cells. Quantification of mature Paneth (*Lyz*<sup>+</sup>) and immature Paneth (*Lyz*<sup>+</sup>/*Muc2*<sup>+</sup>) populations

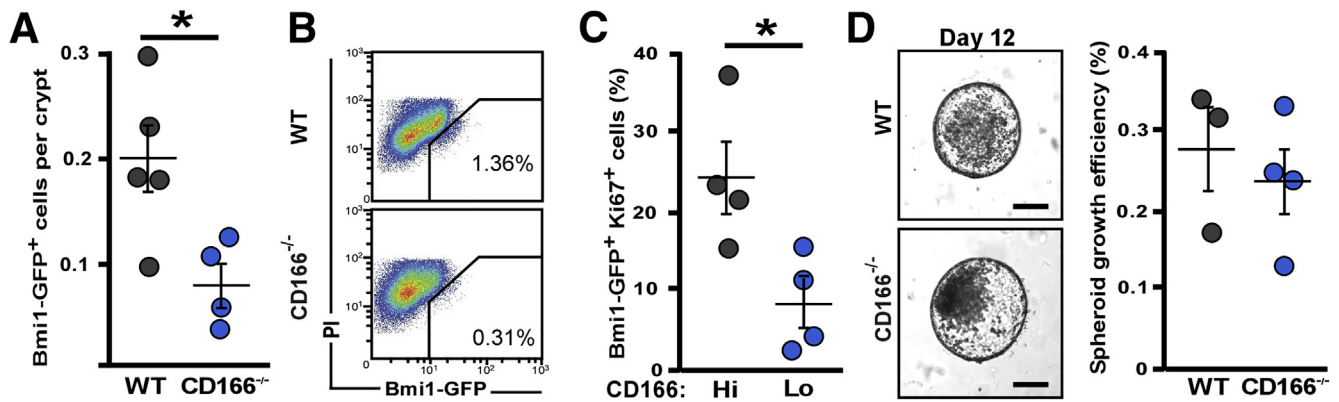


**Figure 5. Loss of CD166 does not lead to compensatory expansion of Bmi1<sup>+</sup> ISCs.** (A) Quantification of Bmi1-GFP<sup>+</sup> cells/crypt in WT (n = 4, gray) and CD166<sup>-/-</sup> (n = 4, blue) tissues by IHC. (B) Flow cytometric analysis of Bmi1-GFP<sup>+</sup> cells from WT (top) or CD166<sup>-/-</sup> (bottom) mice. Experiments were repeated at least 3 times; presented data are from a single representative plot. (C) FACS-isolated Bmi1-GFP<sup>+</sup> cells were subdivided by CD166-expression status from WT mice and stained with antibodies to proliferation marker Ki67 and reveal significantly larger percentage of CD166<sup>+</sup> Bmi1-GFP<sup>+</sup> cells in the cell cycle. (D) FACS-isolated Bmi1-GFP<sup>+</sup> ISCs from WT and CD166<sup>-/-</sup> mice initiated spheroids in culture at similar efficiency. Enteroid images were captured on Leica DMIRB inverted microscope. FACS experiments were performed by using BD Influx cell sorter at OHSU Flow Cytometry Core. Data are representative of experiments repeated at least 3 times. Data are presented as mean  $\pm$  SEM. \**P* < .05. Scale bars = 200  $\mu$ m.

confirmed a significant expansion of immature Paneth cells within the CD166<sup>-/-</sup> crypts (Figure 7F).

To corroborate this finding and to begin exploring a mechanism for inhibition of terminal differentiation, we used correlative light and electron microscopy (CLEM) to rapidly identify Lyz<sup>+</sup> cells by fluorescence, followed by ultrastructural analysis by TEM. By using dual fluorescent and gold particle-conjugated secondary antibodies, the rare bipotential progenitor cells in the upper region of WT crypts were identified as harboring secretory granules containing ultrastructural features of both goblet (mucinous electron transparent regions) and Paneth (large electron dense cores) cell lineages (Figure 9A),<sup>65</sup> whereas mature Paneth cells within the crypt base displayed granules with large electron dense cores (Figure 10A). Importantly and consistent with increased progenitor specification or a block in Paneth cell differentiation, the majority of the CD166<sup>-/-</sup> Paneth cells were progenitor-like cells, even when located in the crypt base (Figure 10B–D, Figure 9B). In addition, expanded analyses revealed heterogeneous Paneth cell differentiation and a spectrum of maturation within a single crypt that spanned granular phenotypes from immature to fully differentiated cells (Figure 9B).

Notably, these immature progenitor-like Paneth cells were often observed within the crypt base, which is unusual because Paneth cells normally undergo terminal differentiation within this high Wnt microenvironment.<sup>23</sup> Therefore, we asked whether loss of CD166 resulted in alterations in pro-growth and differentiation signaling pathways that underscored the stem cell and Paneth cell CD166<sup>-/-</sup> phenotypes. Wnt signaling is the most well-characterized regulatory pathway for intestinal epithelial cell proliferation,<sup>69</sup> with the mature Paneth cell contributing a primary source of Wnt ligands.<sup>1,22</sup> Wnt is also known to regulate Paneth cell maturation,<sup>23</sup> with Paneth cell-derived Wnt3 and

stromal-derived Wnt2b cooperating in maturing these cells.<sup>2</sup> Interestingly, we did not observe a decrease in expression of stromal Wnt2b or antagonistic Wnt5a expression within CD166<sup>-/-</sup> mesenchyme (Figure 11C), supporting that CD166<sup>-/-</sup> epithelia have defects in Wnt signal reception. Therefore, to determine whether the CD166<sup>-/-</sup> Paneth cell differentiation block was associated with reduced Wnt signaling, tissues were stained for active nuclear  $\beta$ -catenin. Although the majority of WT Paneth cells displayed nuclear accumulation of  $\beta$ -catenin, many CD166<sup>-/-</sup> Paneth cells displayed undetectable levels, indicating disruption of Wnt stimulation in these important crypt-based cells within this microenvironment (Figure 11A and B). This observation was further supported by analyses of gene expression in CD166<sup>-/-</sup> relative to WT FACS-isolated crypt epithelium, which indicated downregulation of Wnt target genes *EphB3* and *Mmp7*, two genes that are expressed in Paneth cells (Figure 11C). These data indicate that the loss of CD166 results in disrupted Wnt stimulation, as well as an increased specification of Paneth cells. Wnt signaling has been demonstrated to play a role in Paneth cell terminal differentiation; therefore, diminished Wnt signaling could cause accumulation of immature Paneth cells. However, the Notch signaling pathway is implicated in Paneth cell specification, and perturbation of Notch could also provide an explanation for increased Paneth cell numbers.

Notch signaling, a known regulator of secretory cell specification including Paneth cells,<sup>70</sup> results in an expansion of immature Paneth cells when inhibited.<sup>67,68</sup> Surprisingly, we observed no significant difference in transcriptionally active, cleaved Notch-ICD in CD166<sup>-/-</sup> crypts by IHC<sup>71</sup> or immunoblot analyses (Figure 11D and E). Similarly, we observed no significant difference in expression of Notch ligands (*Dll-1*, *Dll-4*) or target genes (*Hes-1*, *Atoh1*) from CD166<sup>-/-</sup> FACS-isolated



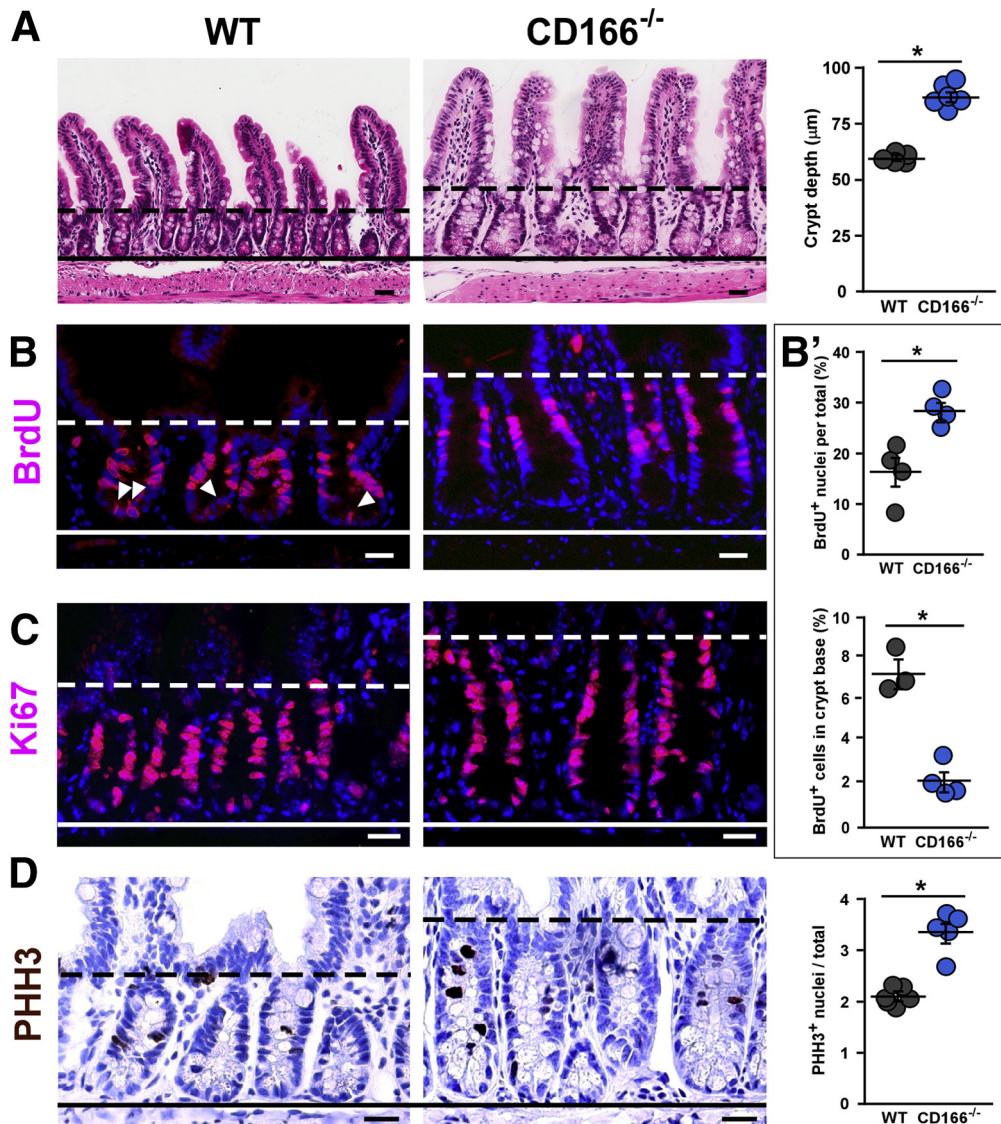


**Figure 6. Expansion of TA zone is accompanied by reduced proliferation within the *Lgr5*<sup>+</sup> stem cell compartment of *CD166*<sup>-/-</sup> crypts.** (A) Low magnification of hematoxylin-eosin-stained WT and *CD166*<sup>-/-</sup> small intestine sections. Images shown are at  $\times 20$ . Morphometric analyses reveal *CD166*<sup>-/-</sup> crypts are deeper than WT controls. Crypt depth analyses conducted in  $n = 6$  mice per genotype with  $n \geq 50$  crypts scored per animal. Cell cycle analyses of WT and *CD166*<sup>-/-</sup> crypts. (B,B') Two-hour BrdU labeling identified expansion of proliferating cells in upper crypt and decrease of BrdU<sup>+</sup> nuclei (red) in *Lgr5* region within *CD166*<sup>-/-</sup> crypts (B, white arrowheads). BrdU analyses were performed on  $n = 4$  mice per genotype, with at least 50 crypts scored per animal. (C) Tissues stained with proliferation marker Ki67 (red) reveal expansion of proliferative crypt compartment within *CD166*<sup>-/-</sup> intestines. (D) *CD166*<sup>-/-</sup> crypts contain more mitotic PHH3<sup>+</sup> cells (brown) per crypt than controls. PHH3 analyses were performed on  $n = 5$  mice per genotype, with at least 25 crypts analyzed per animal. Dashed lines represent upper crypt boundary; solid lines represent lower crypt boundary. Images were captured on Leica DMR upright microscope. Data are presented as mean  $\pm$  SEM. \* $P < .05$ . Scale bars = 25  $\mu$ m.

crypt epithelial cells (Figure 11C and data not shown). However, expression of the Notch target gene, *Olfm4*, was significantly lower in *CD166*<sup>-/-</sup> crypt epithelial cells (Figure 11C), supporting that a subset of Notch targets may be deregulated. These findings indicate that Notch signaling might be more prominent in Paneth cell specification and that Wnt signaling acts in terminal differentiation. Alternatively, it is possible that additional signaling pathways are compromised, or that redundant mechanisms mediated by cell-extracellular matrix

communication also exist to promote tissue homeostasis and prevent disease.<sup>2</sup>

### Enteroids Derived From *CD166*<sup>-/-</sup> Crypts Display Enhanced Budding and Growth

To validate the contribution of *CD166* to ISC homeostasis, we used the in vitro enteroid culture system, which allows for analysis of epithelial-specific ISC regulation within a defined

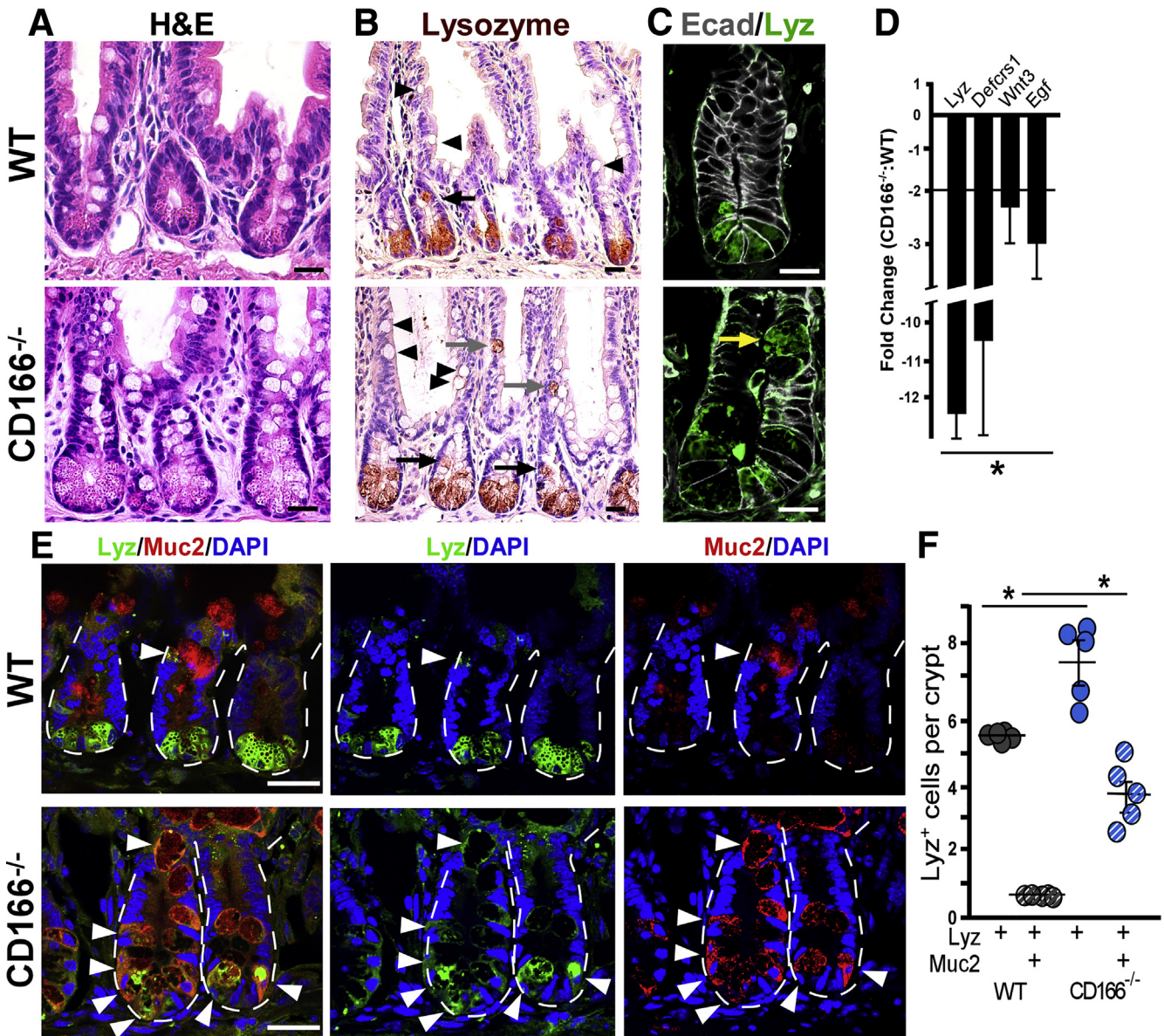


**Figure 7. Disrupted Paneth cell homeostasis in CD166<sup>-/-</sup> crypts.** (A) Hematoxylin-eosin staining of adult WT ( $n = 5$ , upper panel) and CD166<sup>-/-</sup> ( $n = 5$ , lower panel) tissues reveals alterations in Paneth cell morphology within crypt base of CD166<sup>-/-</sup> intestines relative to WT controls. (B) Lysozyme-expressing Paneth cells (brown) are typically nested within crypt base of WT intestines, with occasional progenitor cells detected higher in the crypt (arrow). Goblet cells are scattered throughout the crypt and villus (arrowheads). Paneth cells from CD166<sup>-/-</sup> intestines are expanded within the base of the crypt in size and number and often mislocalized (gray and yellow arrows). (C) E-cadherin (Ecad, white) staining was performed to distinguish individual epithelial cells to facilitate quantification in (F) (WT, gray; CD166<sup>-/-</sup>, blue). (D) Analysis of Paneth cell gene expression from FACS-isolated crypt-based intestinal epithelial cells by qRT-PCR. Data are from at least 3 independent experiments. \* $P < .05$  by 1-sample  $t$  test compared with theoretical mean = -2. (E) WT and CD166<sup>-/-</sup> tissues were co-stained with Lyz (green) and goblet cell marker Muc2 (red) to identify immature Paneth progenitor cells (white arrowheads). A large fraction of Lyz<sup>+</sup> cells within CD166<sup>-/-</sup> tissues are co-labeled with Muc2, even within the crypt base, quantified in (F). Bright field images were captured on Leica DMR upright microscope. Fluorescent images were captured on Olympus BX61 confocal microscope. Data are presented as mean  $\pm$  SEM. \* $P < .05$ . Scale bars = 25  $\mu$ m.

growth factor milieu. This system is touted to bypass the complexity of the in vivo niche where multiple regulatory cues from diverse cell types converge on ISCs to govern their behavior. Cultures initiated from intact crypts provide the platform to assess the Paneth cell competency and to perform rescue experiments for deficiencies within the in vivo

microenvironment. This whole crypt assay surveys the function epithelial niche unit (ie, Paneth cell and ISC), which is different than evaluating the ISC competency, which was assayed by single cell culture experiments in Figures 4F and 5D. It is well-documented that Paneth cells are critical for driving growth, budding, and stem cell maintenance in this



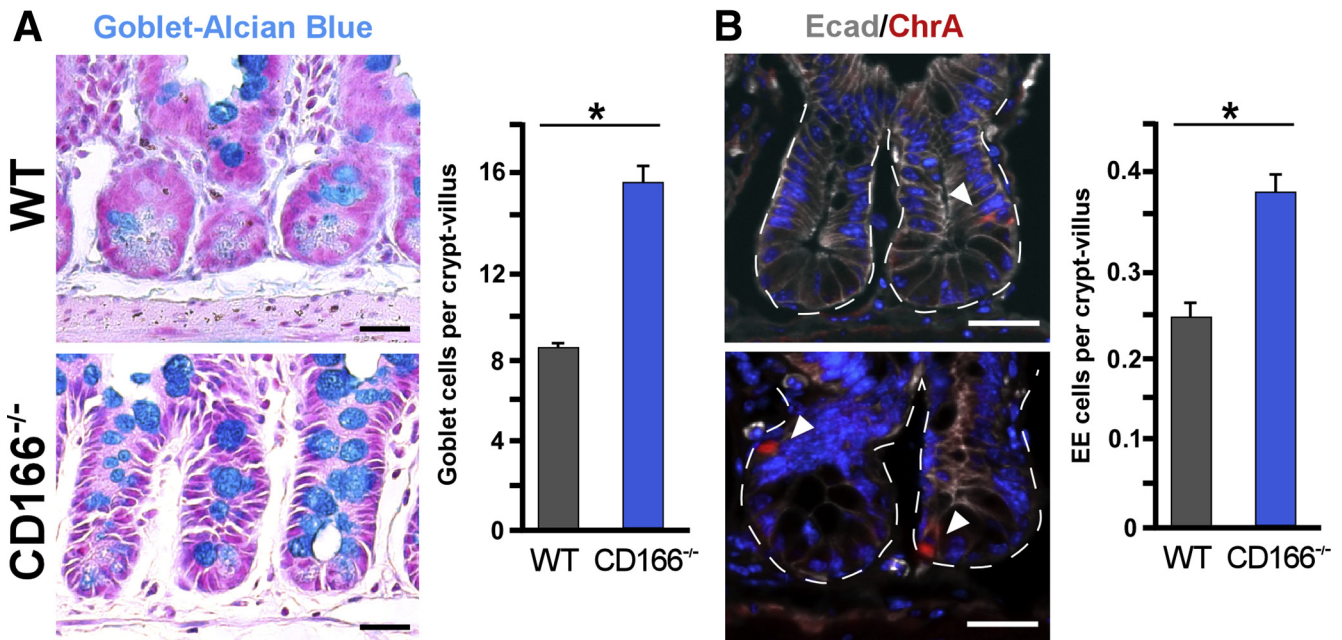


**Figure 8. Secretory lineages are expanded in CD166<sup>-/-</sup> intestinal crypts.** Adult WT ( $n = 3$ ) and CD166<sup>-/-</sup> ( $n = 3$ ) mouse intestines were analyzed for goblet and enteroendocrine cell lineages, with at least 50 crypt/villus units analyzed per mouse. (A) Alcian blue staining revealed expansion of mucinous goblet cells within CD166<sup>-/-</sup> intestines. (B) Enteroendocrine (EE) cells were analyzed by staining with marker chromogranin A (ChrA, red). CD166<sup>-/-</sup> intestines contained increased numbers of ChrA<sup>+</sup> EE cells. Images were captured on Leica DMR upright microscope. Data are presented as mean  $\pm$  SEM. \* $P < .05$ . Scale bars = 25  $\mu$ m.

in vitro system.<sup>1,2,72</sup> Furthermore, under in vitro culture conditions, Rspo1-potentiated Wnt signaling provides an environment analogous to tissue injury or disease states rather than in vivo homeostasis. However, the system can be used to evaluate production of growth factors generated from within the epithelial niche. Therefore, to test whether the CD166<sup>-/-</sup> Paneth cell defect can be rescued in a high Wnt microenvironment and functionally support crypt bud initiation and ISC-driven epithelial growth, crypts were cultured under standard Sato culture conditions.<sup>54</sup> CD166<sup>-/-</sup> crypts initially grew at equivalent rates compared with WT crypts. However, by day 6 in culture, CD166<sup>-/-</sup> crypt-derived enteroids specified more proliferative crypt bud domains and began to grow significantly larger in size (Figure 12A–C, Supplementary Video). Because enteroid budding is driven by Paneth cells,<sup>2</sup> these data demonstrate that exogenous stimulation of the Wnt pathway can rescue defects in Paneth cell maturation to support Lgr5<sup>+</sup> ISC-driven proliferation. This is reflected in the increased number of specified Paneth cells (Figure 7) within CD166<sup>-/-</sup> crypts that are now competent to initiate crypt buds. Furthermore, in this Wnt-stimulated environment, CD166<sup>-/-</sup> crypt-derived enteroids also gained Egf-independent growth. Paneth cells also produce Egf,<sup>1</sup> an important regulatory factor for enteroid growth. Depletion of Egf from the culture medium resulted in a dramatic growth advantage for CD166<sup>-/-</sup> enteroids (Figure 10D and E). Interestingly, withdrawal of the Wnt amplifier, Rspo-1,<sup>73</sup> resulted in collapse of WT and CD166<sup>-/-</sup> enteroids (data not shown). These findings suggest that Paneth cells within enteroids

cannot fully supply Wnt to sustain growth and that increased Paneth cell specification in CD166<sup>-/-</sup> crypt-derived enteroids promote a growth advantage that is enhanced in the absence of Egf. Our analyses of CD166<sup>-/-</sup> Paneth cell competency ex vivo demonstrates that potentiated Wnt signaling rescues the observed in vivo defects in active-cycling stem cell maintenance and points to a function for CD166 in supporting critical cell-cell communication.

## Discussion

Although the cell signaling pathways governing ISC behavior are well-characterized, the role of cell adhesion molecules in shaping the regulatory ISC niche is less clear. Cell adhesion plays important roles in structuring the niche to facilitate productive cell interactions, such as between the Paneth cell and ISC, to mediate cell signals. In other systems, cell adhesion molecules such as syndecans, integrins, and neural cell adhesion molecule have been shown to direct the myriad signals from within the niche to the stem cell.<sup>74,75</sup> In order to maintain the proliferation-to-differentiation gradient responsible for intestinal epithelial homeostasis, productive cell adhesion must balance anchorage of ISCs within the niche with migration of their progeny into different signaling microenvironments. Here we provide evidence that the immunoglobulin-like domain cell adhesion molecule family member CD166/ALCAM participates in the regulation of cell-cell communication to influence ISC maintenance, proliferation, and differentiation within the

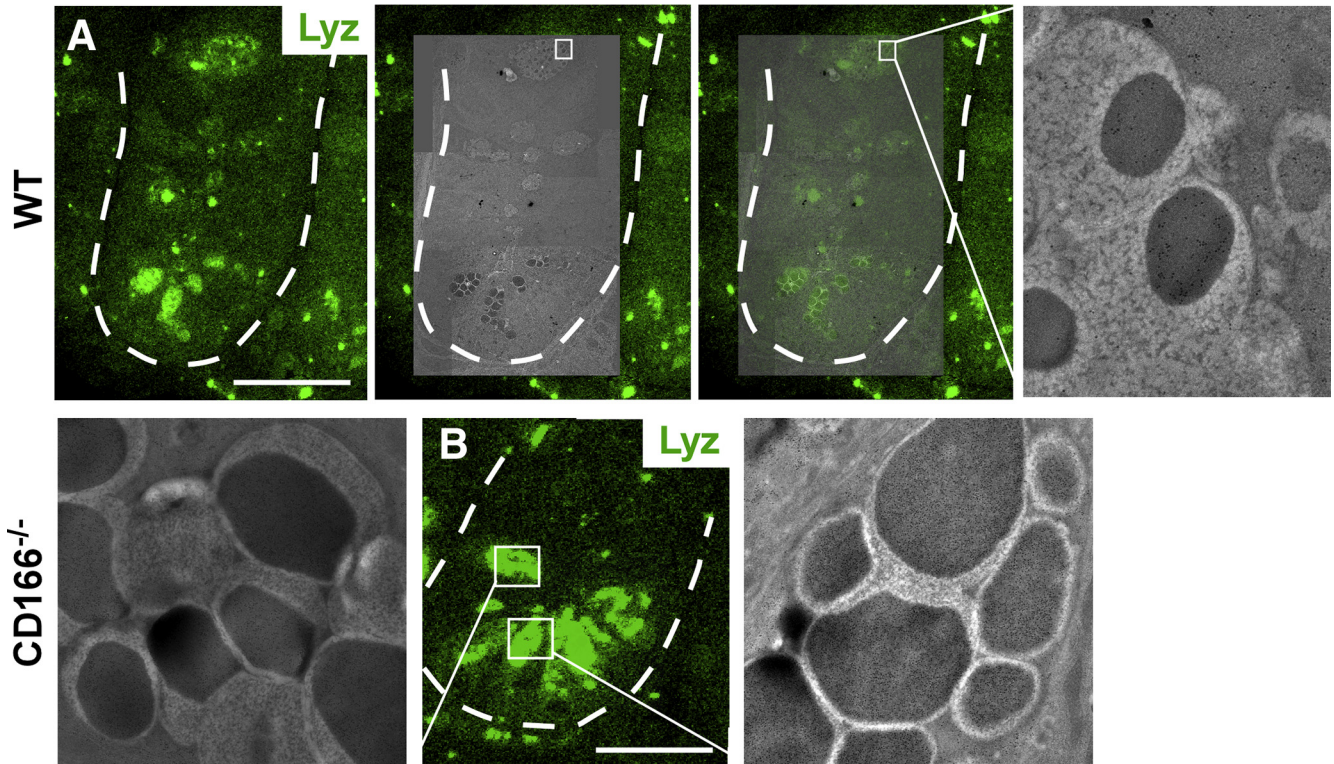


**Figure 9. Granule heterogeneity in  $CD166^{-/-}$  Paneth cells.** CLEM analyses of crypt-based Paneth cell differentiation status in  $CD166^{-/-}$  intestines by granule ultrastructure reveal heterogeneity of differentiation state among cells within a single crypt. (A) Example of rare  $Lyz^{+}$  Paneth progenitor cell identified in WT crypt shows a cell with immature secretory granules containing small electron dense cores surrounded by prominent white mucinous region. (B)  $CD166^{-/-}$  crypt featured in Figure 10 harbors crypt-based Paneth cells with differing differentiation status; top cell is undifferentiated (bottom left TEM image), whereas the bottom cell has mature granules (bottom right TEM image). Images were captured on FEI Tecnai with iCorr integrated fluorescence and TEM at OHSU Multi-Scale Microscopy Core. N = 3 mice per genotype mice were analyzed. Scale bars = 25  $\mu\text{m}$ .

crypt (Figure 13). We investigated the function of CD166 in intestinal epithelial homeostasis by examining crypt cell phenotypes in  $CD166^{-/-}$  mice.

It is important to note that these mice lack CD166 expression within the epithelium and also within the stroma. However, because CD166 functions in both homotypic and heterotypic interactions,<sup>26,41</sup> an epithelial-specific ablation of CD166 would result in loss of both epithelial-epithelial and epithelial-stromal/mesenchymal cell interactions that are reliant on epithelial CD166 expression, likely giving identical phenotypes observed in the total gene knockout mouse. In addition, complete ablation of CD166 may result in phenotypes caused by villus-villus cell disruption, although this is unlikely because epithelial barrier is maintained in  $CD166^{-/-}$  mice (Figure 3). Without studies ablating CD166 in specific stem cell compartments, the described phenotypes cannot be attributed to one cellular relationship over another, but these studies provide important insights in cellular interactions within the intestinal crypt. Furthermore, we selected this mouse model because CD166 has been shown to function in epithelial-epithelial, epithelial-stromal, and stromal-stromal cell interactions.<sup>41</sup> Because of the cellular complexity of the niche, with myriad signaling factors arising from both the adjacent epithelium and underlying

stroma converging to influence behavior of diverse ISC populations, we used this  $CD166^{-/-}$  model to determine whether the restricted expression of CD166 within the ISC zone plays a role in shaping niche signaling and tissue homeostasis.

Here we provide evidence that CD166 shapes the physical niche by mediating the highly ordered spatial positioning between the  $Lgr5^{+}$  ISCs and their Paneth cell neighbors.  $CD166^{-/-}$  crypts displayed disruption of the 1:1 ratio of  $Lgr5^{+}$  ISCs to Paneth cells (Figure 4A and B), skewing the impact of Paneth cell-mediated signaling to the neighboring stem cell, thereby affecting its stem state. The neutral drift hypothesis suggests that  $Lgr5^{+}$  ISCs compete with each other for Paneth cell surface interactions to not only maintain their localization within the crypt base but also to retain stem identity.<sup>61</sup> The hypothesis suggests that ISCs that lose Paneth cell contact will exit the Wnt-influenced zone at the crypt base and become committed progenitors that ultimately differentiate.<sup>61</sup> Notably, loss of CD166 resulted in a reduced pool of  $Lgr5^{+}$  ISCs (25%; Figure 4C) and diminished stem competency and proliferation in the remaining cells (Figures 4F and 6B). This supports that loss of CD166-mediated spatial organization impacted the signaling microenvironment required for stem cell maintenance (Figures 4C-F and 6A-C).



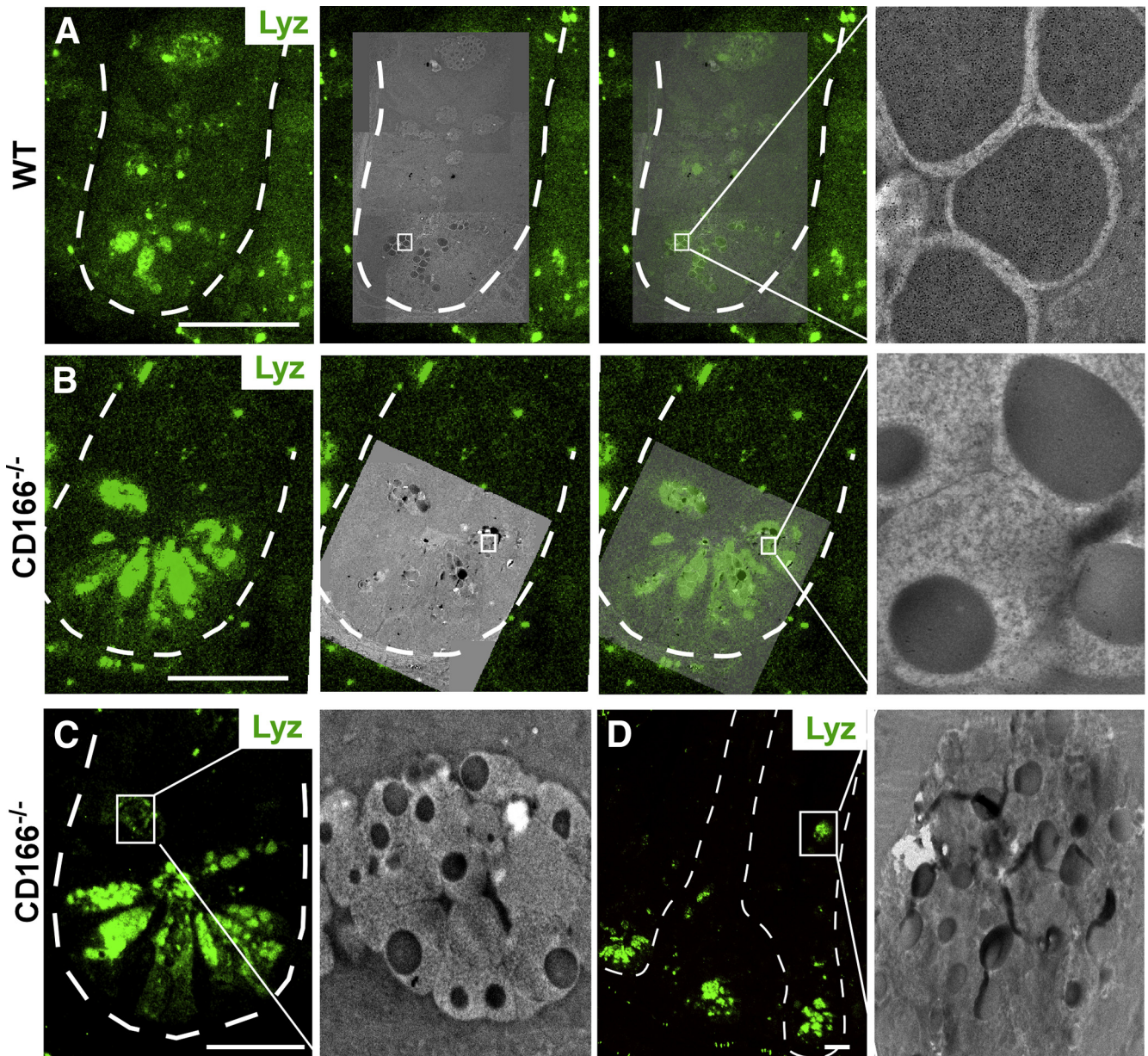


**Figure 10. CD166<sup>-/-</sup> Paneth cells harbor granules with immature ultrastructural features.** Comparison of Paneth cell differentiation status in adult WT ( $n = 3$ ) and CD166<sup>-/-</sup> ( $n = 3$ ) mouse intestinal crypts. Paneth cells were identified by Lyz<sup>+</sup> staining (green), and ultrastructure was analyzed by CLEM. (A) WT Paneth cells (green, top left panel) contain mature granules with large electron-dense cores (dark gray), surrounded by scant electron transparent mucinous halos (light gray, TEM image in top right panel). (B) CD166<sup>-/-</sup> Paneth cells (middle panel) are most often immature, displaying smaller electron-dense cores and more prominent mucinous domains. (C) Identification of immature Paneth progenitors in mid-crypt of CD166<sup>-/-</sup> tissues. (D) Identification of mislocalized Lyz<sup>+</sup> cell on the villus of CD166<sup>-/-</sup> tissue section, displaying small electron-dense cores and large mucinous domains. Majority of Paneth cell granules from CD166<sup>-/-</sup> mouse intestines display an immature cell phenotype. All studies were repeated in at least  $n = 3$  mice. Six to 8 crypts from each mouse were analyzed. Images were captured on FEI Tecnai with iCorr integrated fluorescence and TEM at OHSU Multi-Scale Microscopy Core. Scale bars = 25  $\mu\text{m}$ .

Despite the reduction of Lgr5<sup>+</sup> ISCs, an alternative homeostatic set point was established that supported functionality of the intestine. In numerous injury contexts resulting in depletion of active-cycling ISCs, the slow-cycling Bmi1<sup>+</sup> ISC population expands in a compensatory manner to reconstitute the active-cycling stem cell population.<sup>10,11,15</sup> Unexpectedly we detected an overall reduction

of the Bmi1<sup>+</sup> ISC population (Figure 5A and B). It is possible that reduced Bmi1<sup>+</sup> ISC numbers result from the minor decrease in Notch signaling (Figure 11C), because Bmi1<sup>+</sup> ISCs were recently reported to function downstream of Notch.<sup>76</sup> An alternative explanation might revolve around the observation that the minor subset of Bmi1<sup>+</sup> ISCs that are CD166<sup>hi</sup> are more proliferative (Figure 5C). In this instance



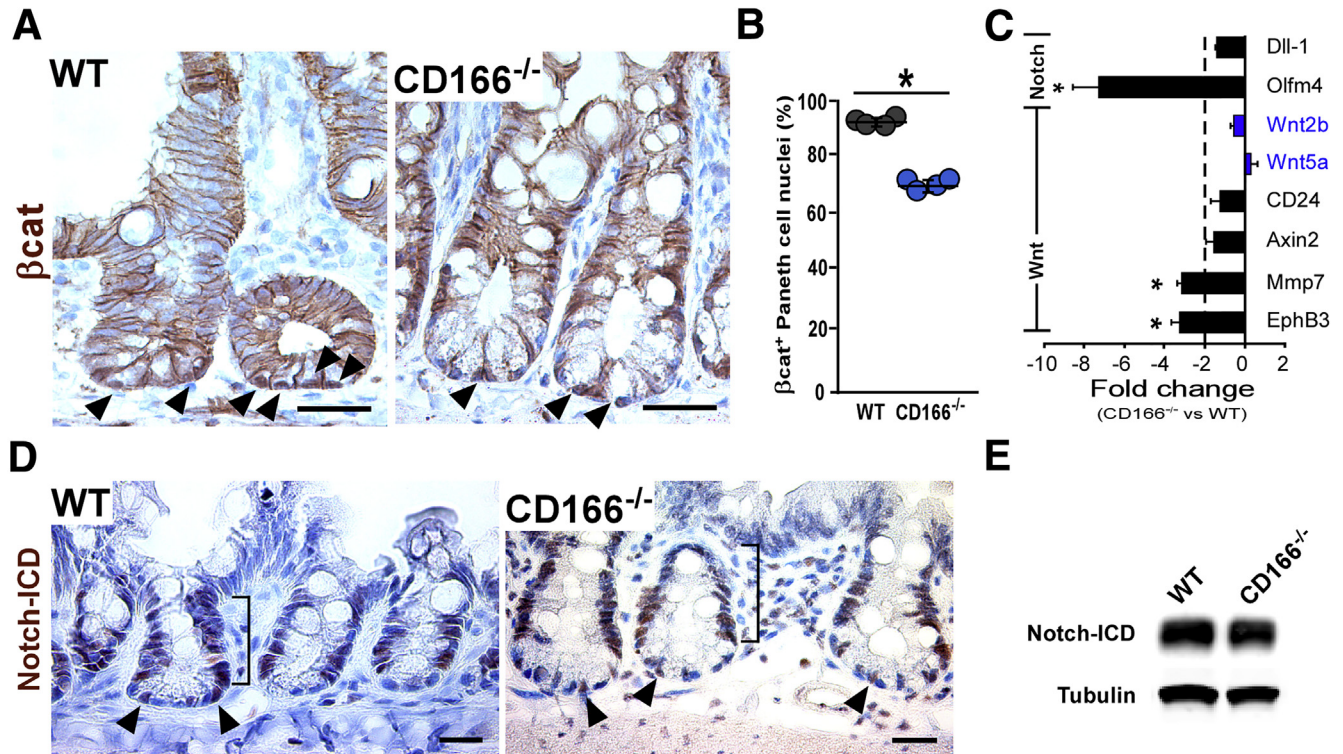


**Figure 11. Diminished Wnt and Notch signaling within CD166<sup>-/-</sup> crypts.** (A) WT (n = 4) and CD166<sup>-/-</sup> (n = 4) tissues were analyzed for nuclear  $\beta$ -catenin staining (brown) as a readout for Wnt signaling by IHC. Although the majority of WT Paneth cells displayed nuclear accumulation of  $\beta$ -catenin (arrowheads), significantly fewer CD166<sup>-/-</sup> Paneth stains showed detectable nuclear  $\beta$ -catenin signal, quantified in (B). (C) Analysis of Wnt and Notch target gene expression from FACS-isolated intestinal crypt-based epithelial cells (black bars) or mesenchyme enriched fractions (blue bars) by qRT-PCR. \* $P < .05$  by 1-sample  $t$  test compared with theoretical mean = -2. Data are from at least 3 independent experiments. Analysis of Notch signaling pathway by (D) IHC and Western blotting (E) for Notch intracellular domain (ICD) in WT and CD166<sup>-/-</sup> crypts. Bright field images were captured on Leica DMR upright microscope. Data are representative of experiments repeated at least 3 times. Data are presented as mean  $\pm$  SEM. \* $P < .05$ . Scale bars = 25  $\mu$ m.

our findings might indicate that the largely Wnt-independent Bmi1<sup>+</sup> ISC population<sup>8,11</sup> functionally expresses CD166 as it transitions into a proliferative state (Figure 5C). This putative mechanistic transition into a Wnt-responsive state could explain how Bmi1<sup>+</sup> ISCs become poised to proliferate and compensate for loss of active-cycling Lgr5<sup>+</sup> ISCs in response to injury (Figure 13A). It would also explain how loss of CD166 could result in decreased Bmi1<sup>+</sup> cell numbers, because Ki67-positive Bmi1 ISCs in the CD166<sup>-/-</sup> intestines were not readily identified (not shown). This indicates that loss of Lgr5<sup>+</sup> ISCs is not compensated by the Bmi1<sup>+</sup> ISC population but by expansion of another cellular pool.

The TA cell population represents one candidate population that can compensate for Lgr5<sup>+</sup> ISC depletion to maintain epithelial homeostasis. CD166 ablation resulted in enhanced TA cell numbers and proliferative activity (Figure 6B–D). This concept is supported by the demonstration that coordinated control of differentiation, proliferation, and death functions to maintain overall cell census.<sup>77</sup> TA zone expansion is also consistent with the neutral drift hypothesis, where unsupported Lgr5<sup>+</sup> ISCs

cannot maintain stemness.<sup>61</sup> In this scenario, Lgr5-expressing cells that migrate away from the Wnt ligand sources at the base of the crypt, which are derived in Paneth and stromal cells, expand the pool of epithelial progenitors. In the context of injury (ie, radiation or chemotherapy) and active-cycling ISC loss, a similar TA compartment expansion has been reported.<sup>10,52,64</sup> Therefore, expansion of the TA zone in CD166<sup>-/-</sup> crypts is likely due to defective maintenance of the Lgr5<sup>+</sup> ISC population that is associated with reduction of Wnt-mediated signaling. We report that Wnt-associated genes are downregulated (Figures 4 and 11). That the TA and ISC populations differentially respond to Wnt signals is not unprecedented, because it is known that discrete ISC populations, as well as downstream progenitor cells, respond to different proliferative signaling cues.<sup>78</sup> For example, Wnt signaling targets the active-cycling ISC population because nuclear  $\beta$ -catenin is found in these cells, yet nuclear  $\beta$ -catenin is absent in the TA zone (Figure 11A). These differences likely underlie the differential injury response within the stem cell and TA compartments,<sup>10,64,79</sup> as well as point to alternative paths for safeguarding “homeostasis” when one ISC population is compromised.



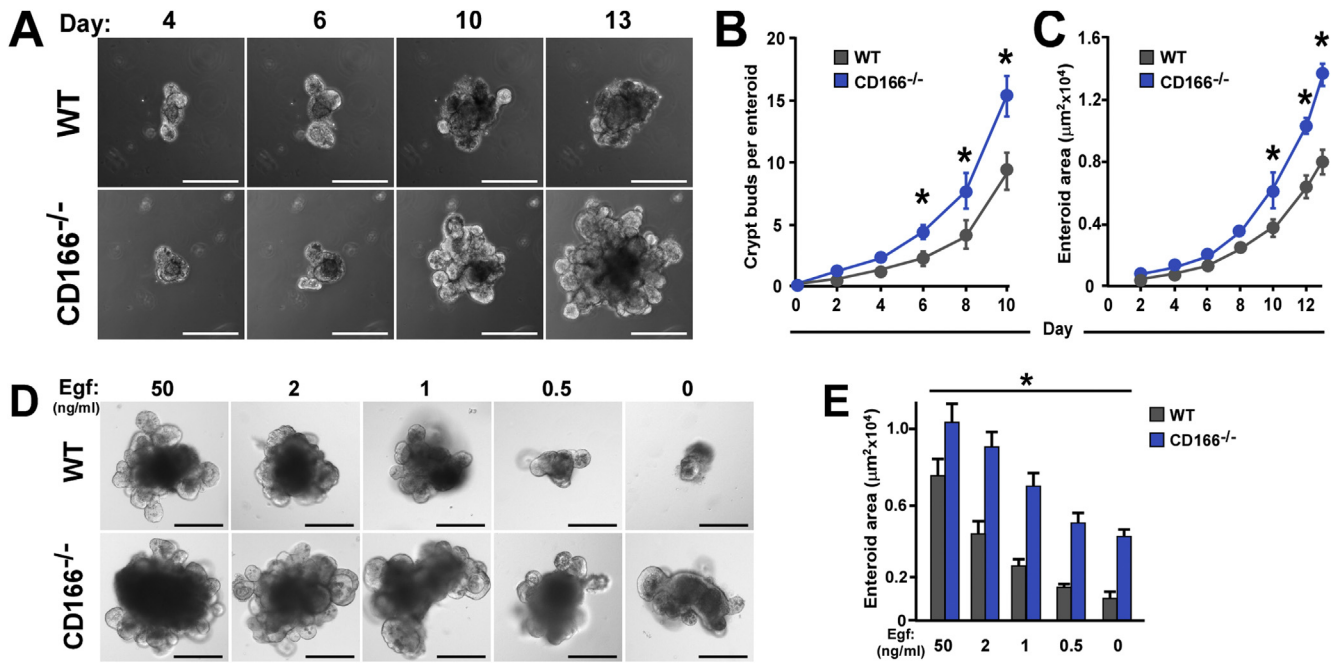


**Figure 12. CD166 loss results in aberrant enteroid growth.** (A) Representative time course of intestinal enteroids cultured from isolated crypts from adult WT ( $n = 5$ ) and CD166<sup>-/-</sup> ( $n = 5$ ) mice. CD166<sup>-/-</sup> enteroids specified more proliferative crypt bud domains (B) displayed more rapid growth (C) by 10 days compared with WT enteroids. (D) CD166<sup>-/-</sup> enteroids cultured in presence of diminished exogenous Egf have significant growth advantage compared with WT controls, quantified in (E). Data are representative of experiments that were repeated at least 3 times, with at least  $n = 10$  enteroids per condition/time point scored. Images were captured on Leica DMIRB inverted microscope. Data are presented as mean  $\pm$  SEM. \* $P < .05$ . Scale bars = 200  $\mu\text{m}$ .

The unsupported CD166<sup>-/-</sup> Lgr5<sup>+</sup> ISCs were associated with diminished Wnt ligand expression in the neighboring Paneth cells (Figure 7D). Because Wnt3 ligand is a Paneth cell differentiation product, this indicates that Paneth cell

maturation was blocked. Wnt signaling has known roles in Paneth cells, promoting their localization within the high Wnt environment at the crypt base<sup>80</sup> and driving terminal lineage differentiation by regulating expression of

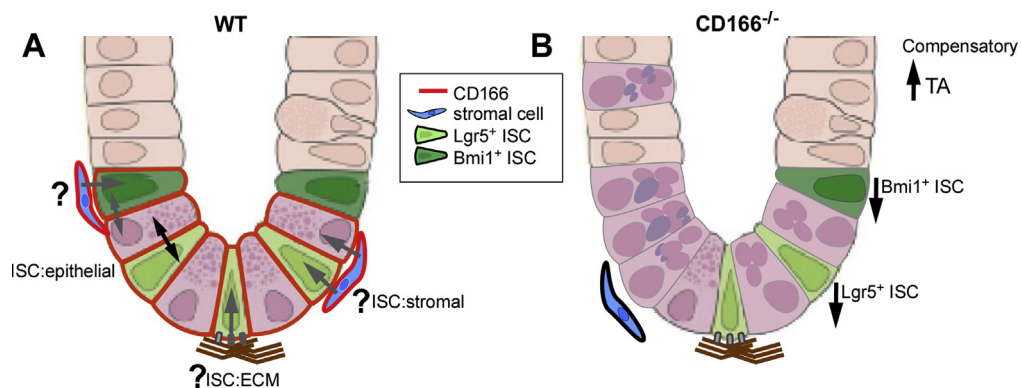


**Figure 13. Multifaceted CD166-mediated regulatory function within the ISC niche.** Cartoon depiction of CD166 function within ISC niche. (A) CD166-expressing cells (either epithelial or mesenchymal, outlined in red) function to mediate communication between ISC:epithelial and likely ISC:stromal cell and possibly ISC:extracellular matrix to coordinate regulatory signaling within the ISC niche. Active-cycling Lgr5<sup>+</sup> ISCs (light green) receive inputs from neighboring Paneth (pink) and underlying stromal cell populations to regulate stem cell proliferation and differentiation. A subset of Bmi1<sup>+</sup> ISCs (dark green) express CD166, which may poise them to transition from slow-cycling to active-cycling ISC state. (B) In CD166<sup>-/-</sup> intestines, the Wnt microenvironment is impaired, deregulating both Paneth cell homeostasis and leading to reduced pools of active and slow-cycling ISCs (Lgr5<sup>+</sup> and Bmi1<sup>+</sup> populations, respectively). Both active-cycling, Lgr5<sup>+</sup> ISC (light green) and slow-cycling, Bmi1<sup>+</sup> ISC (dark green) are impacted by CD166 depletion, along with compensatory expansion of TA compartment.

differentiated Paneth cell genes including *Wnt3*, *Mmp7*, and *Defensins*.<sup>2,23,81–83</sup> The observed Paneth cell differentiation defect occurred in conjunction with diminished expression of Wnt target genes and decreased nuclear  $\beta$ -catenin (Figure 11B and C). This immature phenotype was confirmed by revealing phenotypes associated with bipotential secretory progenitor cells (Figures 7, 9, and 10). Interestingly, numbers of these immature progenitors were increased in *CD166*<sup>-/-</sup> intestines (Figure 7F). This was consistent with increased specification of the lineage that has been previously described to be Notch signaling-mediated.<sup>66,68,70,83</sup> In the *CD166*-null crypts, Notch signaling is mildly depressed (Figure 11C). It is possible that a *CD166*<sup>-/-</sup> mediated alternative homeostatic set point is established in response to depressed Wnt signaling that blocks Paneth cell terminal differentiation. This block in differentiation may in turn stimulate a Notch-mediated increase in specification of the Paneth cell lineage to increase numbers of Wnt ligand producing cells in the stem cell niche. Notably, *CD166*<sup>-/-</sup> intestines phenocopied Notch inhibition, yet Paneth and ISCs retained expression of the epithelial ligands (Figure 11C), highlighting the requirement for productive cell-cell contact to support efficient Notch signal transduction. A *CD166*-deficient environment compromises overall stem cell maintenance.

Different types of cell adhesion exist along the crypt-villus axis and likely regulate distinct epithelial programs to influence the proliferation to differentiation axis as cells migrate from the crypt niche. *CD166* is highly expressed in the base of the crypt, and our data indicate that it functions to mediate cell signaling cues. A cellular mechanism for *CD166* function within the crypt is bringing cells in close proximity to facilitate cellular communication. A molecular mechanism may be through its association with adherens junctions,<sup>60</sup> because these complexes are actively linked to Wnt pathway regulation<sup>84</sup> and mediate other cell-cell regulatory nodes (Figure 13). Furthermore, *CD166* is a target of non-canonical Wnt signaling, which is known to regulate the canonical Wnt pathway,<sup>49</sup> and provides a link to the coordinated regulation between the non-canonical (mediated through *Wnt5A*) and canonical Wnt signaling pathways within the crypt base. It is feasible that these mechanisms coordinate the *CD166* influence on ISC regulation within the niche.

Although our study indicates that *CD166* mediates cell-cell communication between ISC and adjacent epithelial cells, additional *CD166*-mediated interactions may exist. *CD166* is heavily localized to the basolateral surface of both ISC and Paneth cells (Figure 2), as well as a number of cells within the surrounding mesenchyme, including macrophages<sup>85</sup> and fibroblasts. In addition, *CD6*, expressed on T cells, is a known heterotypic binding partner.<sup>38–40</sup> It is possible that ISC and Paneth cell expression of *CD166* facilitates interactions between these cells and the underlying stroma. *CD166*-mediated ISC-stromal cell communication might provide one possible explanation for the observation that *CD166*<sup>-/-</sup> associated Paneth cell differentiation defects may not be rescued by expression of stromal Wnt ligands, because their expression levels are not altered in these

intestines (Figure 11C). Previous studies have demonstrated that deletion of *Wnt3* in Paneth cells is compensated by Wnt ligands within the stroma,<sup>2</sup> including *Foxl1*-expressing mesenchymal cells.<sup>3</sup> Therefore, it is possible that a cell adhesion-mediated reception of these signals is functionally required. This suggests an additional intriguing *CD166*-mediated regulatory pathway underlying ISC homeostasis (Figure 13).

## Conclusions

The conserved cell adhesion molecule *CD166* defines a tight spatial domain in the active-cycling ISC zone composed of Paneth cells and *Lgr5*<sup>+</sup> ISCs. Analyses of the active-cycling stem cell domain in *CD166*<sup>-/-</sup> mice revealed a defect in stem cell maintenance and function, which is due in part to a block in terminal differentiation of the Paneth cell, an important source of Wnt ligands. Our study indicates a role for *CD166* in maintaining the structure of the ISC niche by mediating cell-cell communication on multiple fronts (ISC-epithelial, undiscovered roles in ISC-stromal and ISC-extracellular matrix interactions; Figure 13A and B) to support stem cell maintenance, proliferation, and differentiation. Understanding this important regulatory axis has translational value, because *CD166* is highly expressed on cancer cells from patients with poor prognoses.<sup>86</sup> Clearly, a regulatory node that senses cues from its microenvironment on multiple fronts to direct stem cell function is an attractive access point for possible therapeutic intervention.

## References

1. Sato T, van Es JH, Snippert HJ, et al. Paneth cells constitute the niche for *Lgr5* stem cells in intestinal crypts. *Nature* 2011;469:415–418.
2. Farin HF, Van Es JH, Clevers H. Redundant sources of Wnt regulate intestinal stem cells and promote formation of Paneth cells. *Gastroenterology* 2012;143:1518–1529 e7.
3. Aoki R, Shoshkes-Carmel M, Gao N, et al. *Foxl1*-expressing mesenchymal cells constitute the intestinal stem cell niche. *Cell Mol Gastroenterol Hepatol* 2016;2:175–188.
4. Barker N, van Es JH, Kuipers J, et al. Identification of stem cells in small intestine and colon by marker gene *Lgr5*. *Nature* 2007;449:1003–1007.
5. Basak O, van de Born M, Korving J, et al. Mapping early fate determination in *Lgr5*<sup>+</sup> crypt stem cells using a novel *Ki67*-RFP allele. *EMBO J* 2014;33:2057–2068.
6. Cheng H, Leblond CP. Origin, differentiation and renewal of the four main epithelial cell types in the mouse small intestine: V—unitarian theory of the origin of the four epithelial cell types. *Am J Anat* 1974;141:537–561.
7. Li L, Clevers H. Coexistence of quiescent and active adult stem cells in mammals. *Science* 2010;327:542–545.
8. Sangiorgi E, Capecchi MR. *Bmi1* is expressed in vivo in intestinal stem cells. *Nat Genet* 2008;40:915–920.

9. Montgomery RK, Carlone DL, Richmond CA, et al. Mouse telomerase reverse transcriptase (mTert) expression marks slowly cycling intestinal stem cells. *Proc Natl Acad Sci U S A* 2011;108:179–184.
10. Tian H, Biehs B, Warming S, et al. A reserve stem cell population in small intestine renders Lgr5-positive cells dispensable. *Nature* 2011;478:255–259.
11. Yan KS, Chia LA, Li X, et al. The intestinal stem cell markers Bmi1 and Lgr5 identify two functionally distinct populations. *Proc Natl Acad Sci U S A* 2012;109:466–471.
12. Buczaccki SJ, Zecchini HI, Nicholson AM, et al. Intestinal label-retaining cells are secretory precursors expressing Lgr5. *Nature* 2013;495:65–69.
13. Tetteh PW, Basak O, Farin HF, et al. Replacement of lost Lgr5-positive stem cells through plasticity of their enterocyte-lineage daughters. *Cell Stem Cell* 2016;18:203–213.
14. van Es JH, Sato T, van de Wetering M, et al. Dll1+ secretory progenitor cells revert to stem cells upon crypt damage. *Nat Cell Biol* 2012;14:1099–1104.
15. Smith NR, Gallagher AC, Wong MH. Defining a stem cell hierarchy in the intestine: markers, caveats and controversies. *J Physiol* 2016;594:4781–4790.
16. Barker N, Clevers H. Tracking down the stem cells of the intestine: strategies to identify adult stem cells. *Gastroenterology* 2007;133:1755–1760.
17. Kim TH, Li F, Ferreiro-Neira I, et al. Broadly permissive intestinal chromatin underlies lateral inhibition and cell plasticity. *Nature* 2014;506:511–515.
18. Biswas S, Davis H, Irshad S, et al. Microenvironmental control of stem cell fate in intestinal homeostasis and disease. *J Pathol* 2015;237:135–145.
19. Medema JP, Vermeulen L. Microenvironmental regulation of stem cells in intestinal homeostasis and cancer. *Nature* 2011;474:318–326.
20. Booth C, Potten CS. Gut instincts: thoughts on intestinal epithelial stem cells. *J Clin Invest* 2000;105:1493–1499.
21. Brittan M, Wright NA. Gastrointestinal stem cells. *J Pathol* 2002;197:492–509.
22. Gregorieff A, Pinto D, Begthel H, et al. Expression pattern of Wnt signaling components in the adult intestine. *Gastroenterology* 2005;129:626–638.
23. van Es JH, Jay P, Gregorieff A, et al. Wnt signalling induces maturation of Paneth cells in intestinal crypts. *Nat Cell Biol* 2005;7:381–386.
24. Smith NR, Davies PS, Silk AD, et al. Epithelial and mesenchymal contribution to the niche: a safeguard for intestinal stem cell homeostasis. *Gastroenterology* 2012;143:1426–1430.
25. Jenkins AB, McCaffery JM, Van Doren M. Drosophila E-cadherin is essential for proper germ cell-soma interaction during gonad morphogenesis. *Development* 2003;130:4417–4426.
26. Levin TG, Powell AE, Davies PS, et al. Characterization of the intestinal cancer stem cell marker CD166 in the human and mouse gastrointestinal tract. *Gastroenterology* 2010;139:2072–2082 e5.
27. Marthiens V, Kazanis I, Moss L, et al. Adhesion molecules in the stem cell niche: more than just staying in shape? *J Cell Sci* 2010;123:1613–1622.
28. McEwen AE, Escobar DE, Gottardi CJ. Signaling from the adherens junction. *Subcell Biochem* 2012;60:171–196.
29. Bowen MA, Patel DD, Li X, et al. Cloning, mapping, and characterization of activated leukocyte-cell adhesion molecule (ALCAM), a CD6 ligand. *J Exp Med* 1995;181:2213–2220.
30. Whitney GS, Starling GC, Bowen MA, et al. The membrane-proximal scavenger receptor cysteine-rich domain of CD6 contains the activated leukocyte cell adhesion molecule binding site. *J Biol Chem* 1995;270:18187–18190.
31. Cho RW, Clarke MF. Recent advances in cancer stem cells. *Curr Opin Genet Dev* 2008;18:48–53.
32. Hassan NJ, Simmonds SJ, Clarkson NG, et al. CD6 regulates T-cell responses through activation-dependent recruitment of the positive regulator SLP-76. *Mol Cell Biol* 2006;26:6727–6738.
33. Ikeda K, Quertermous T. Molecular isolation and characterization of a soluble isoform of activated leukocyte cell adhesion molecule that modulates endothelial cell function. *J Biol Chem* 2004;279:55315–55323.
34. Jezierska A, Matysiak W, Motyl T. ALCAM/CD166 protects breast cancer cells against apoptosis and autophagy. *Med Sci Monit* 2006;12:BR263–BR273.
35. Kato Y, Tanaka Y, Hayashi M, et al. Involvement of CD166 in the activation of human gamma delta T cells by tumor cells sensitized with nonpeptide antigens. *J Immunol* 2006;177:877–884.
36. Masedunskas A, King JA, Tan F, et al. Activated leukocyte cell adhesion molecule is a component of the endothelial junction involved in transendothelial monocyte migration. *FEBS Lett* 2006;580:2637–2645.
37. Ohneda O, Ohneda K, Arai F, et al. ALCAM (CD166): its role in hematopoietic and endothelial development. *Blood* 2001;98:2134–2142.
38. Bowen MA, Bajorath J, D'Egidio M, et al. Characterization of mouse ALCAM (CD166): the CD6-binding domain is conserved in different homologs and mediates cross-species binding. *Eur J Immunol* 1997;27:1469–1478.
39. Kanki JP, Chang S, Kuwada JY. The molecular cloning and characterization of potential chick DM-GRASP homologs in zebrafish and mouse. *J Neurobiol* 1994;25:831–845.
40. Patel DD, Wee SF, Whichard LP, et al. Identification and characterization of a 100-kD ligand for CD6 on human thymic epithelial cells. *J Exp Med* 1995;181:1563–1568.
41. Degen WG, van Kempen LC, Gijzen EG, et al. MEMD, a new cell adhesion molecule in metastasizing human melanoma cell lines, is identical to ALCAM (activated leukocyte cell adhesion molecule). *Am J Pathol* 1998;152:805–813.
42. Corbel C, Cormier F, Pourquie O, et al. BEN, a novel surface molecule of the immunoglobulin superfamily on avian hemopoietic progenitor cells shared with neural cells. *Exp Cell Res* 1992;203:91–99.
43. Uchida N, Yang Z, Combs J, et al. The characterization, molecular cloning, and expression of a novel

- hematopoietic cell antigen from CD34+ human bone marrow cells. *Blood* 1997;89:2706–2716.
44. Arai F, Ohneda O, Miyamoto T, et al. Mesenchymal stem cells in perichondrium express activated leukocyte cell adhesion molecule and participate in bone marrow formation. *J Exp Med* 2002;195:1549–1563.
  45. Bruder SP, Ricalton NS, Boynton RE, et al. Mesenchymal stem cell surface antigen SB-10 corresponds to activated leukocyte cell adhesion molecule and is involved in osteogenic differentiation. *J Bone Miner Res* 1998;13:655–663.
  46. Dalerba P, Dylla SJ, Park IK, et al. Phenotypic characterization of human colorectal cancer stem cells. *Proc Natl Acad Sci U S A* 2007;104:10158–10163.
  47. Chitteti BR, Kobayashi M, Cheng Y, et al. CD166 regulates human and murine hematopoietic stem cells and the hematopoietic niche. *Blood* 2014;124:519–529.
  48. Prieve MG, Moon RT. Stromelysin-1 and mesothelin are differentially regulated by Wnt-5a and Wnt-1 in C57mg mouse mammary epithelial cells. *BMC Dev Biol* 2003;3:2.
  49. Moon RT, Kohn AD, De Ferrari GV, et al. WNT and beta-catenin signalling: diseases and therapies. *Nat Rev Genet* 2004;5:691–701.
  50. Hosen N, Yamane T, Muijtjens M, et al. Bmi-1-green fluorescent protein-knock-in mice reveal the dynamic regulation of bmi-1 expression in normal and leukemic hematopoietic cells. *Stem Cells* 2007;25:1635–1644.
  51. Weiner JA, Koo SJ, Nicolas S, et al. Axon fasciculation defects and retinal dysplasias in mice lacking the immunoglobulin superfamily adhesion molecule BEN/ALCAM/SC1. *Mol Cell Neurosci* 2004;27:59–69.
  52. Davies PS, Dismuke AD, Powell AE, et al. Wnt-reporter expression pattern in the mouse intestine during homeostasis. *BMC Gastroenterol* 2008;8:57.
  53. Magness ST, Puthoff BJ, Crissey MA, et al. A multicenter study to standardize reporting and analyses of fluorescence-activated cell-sorted murine intestinal epithelial cells. *Am J Physiol Gastrointest Liver Physiol* 2013;305:G542–G551.
  54. Sato T, Vries RG, Snippert HJ, et al. Single Lgr5 stem cells build crypt-villus structures in vitro without a mesenchymal niche. *Nature* 2009;459:262–265.
  55. Wang F, Scoville D, He XC, et al. Isolation and characterization of intestinal stem cells based on surface marker combinations and colony-formation assay. *Gastroenterology* 2013;145:383–395, e1–21.
  56. Sumagin R, Robin AZ, Nusrat A, et al. Transmigrated neutrophils in the intestinal lumen engage ICAM-1 to regulate the epithelial barrier and neutrophil recruitment. *Mucosal Immunol* 2014;7:905–915.
  57. Wong MH, Rubinfeld B, Gordon JL. Effects of forced expression of an NH2-terminal truncated beta-catenin on mouse intestinal epithelial homeostasis. *J Cell Biol* 1998;141:765–777.
  58. Slot JW, Geuze HJ. Cryosectioning and immunolabeling. *Nat Protoc* 2007;2:2480–2491.
  59. Keene DR, Tufa SF, Wong MH, et al. Correlation of the same fields imaged in the TEM, confocal, LM, and microCT by image registration: from specimen preparation to displaying a final composite image. *Methods Cell Biol* 2014;124:391–417.
  60. Tomita K, van Bokhoven A, Jansen CF, et al. Coordinate recruitment of E-cadherin and ALCAM to cell-cell contacts by alpha-catenin. *Biochem Biophys Res Commun* 2000;267:870–874.
  61. Snippert HJ, van der Flier LG, Sato T, et al. Intestinal crypt homeostasis results from neutral competition between symmetrically dividing Lgr5 stem cells. *Cell* 2010;143:134–144.
  62. Munoz J, Stange DE, Schepers AG, et al. The Lgr5 intestinal stem cell signature: robust expression of proposed quiescent '+4' cell markers. *Embo J* 2012;31:3079–3091.
  63. Ritsma L, Ellenbroek SI, Zomer A, et al. Intestinal crypt homeostasis revealed at single-stem-cell level by in vivo live imaging. *Nature* 2014;507:362–365.
  64. King SL, Mohiuddin JJ, Dekaney CM. Paneth cells expand from newly created and preexisting cells during repair after doxorubicin-induced damage. *Am J Physiol Gastrointest Liver Physiol* 2013;305:G151–G162.
  65. Troughton WD, Trier JS. Paneth and goblet cell renewal in mouse duodenal crypts. *J Cell Biol* 1969;41:251–268.
  66. Cheng H. Origin, differentiation and renewal of the four main epithelial cell types in the mouse small intestine: IV—Paneth cells. *Am J Anat* 1974;141:521–535.
  67. Tsai YH, VanDussen KL, Sawey ET, et al. ADAM10 regulates Notch function in intestinal stem cells of mice. *Gastroenterology* 2014;147:822–834 e13.
  68. VanDussen KL, Carulli AJ, Keeley TM, et al. Notch signaling modulates proliferation and differentiation of intestinal crypt base columnar stem cells. *Development* 2012;139:488–497.
  69. Pinto D, Gregorieff A, Begthel H, et al. Canonical Wnt signals are essential for homeostasis of the intestinal epithelium. *Genes Dev* 2003;17:1709–1713.
  70. Noah TK, Shroyer NF. Notch in the intestine: regulation of homeostasis and pathogenesis. *Annu Rev Physiol* 2013;75:263–288.
  71. Tian H, Biehs B, Chiu C, et al. Opposing activities of Notch and Wnt signaling regulate intestinal stem cells and gut homeostasis. *Cell Rep* 2015;11:33–42.
  72. Durand A, Donahue B, Peignon G, et al. Functional intestinal stem cells after Paneth cell ablation induced by the loss of transcription factor Math1 (Atoh1). *Proc Natl Acad Sci U S A* 2012;109:8965–8970.
  73. de Lau W, Barker N, Low TY, et al. Lgr5 homologues associate with Wnt receptors and mediate R-spondin signalling. *Nature* 2011;476:293–297.
  74. Beauvais DM, Rapraeger AC. Syndecans in tumor cell adhesion and signaling. *Reprod Biol Endocrinol* 2004;2:3.
  75. Lustig KD, Kirschner MW. Use of an oocyte expression assay to reconstitute inductive signaling. *Proc Natl Acad Sci U S A* 1995;92:6234–6238.
  76. Lopez-Arribillaga E, Rodilla V, Pellegrinet L, et al. Bmi1 regulates murine intestinal stem cell proliferation and self-renewal downstream of Notch. *Development* 2015;142:41–50.



77. Hermiston ML, Wong MH, Gordon JI. Forced expression of E-cadherin in the mouse intestinal epithelium slows cell migration and provides evidence for nonautonomous regulation of cell fate in a self-renewing system. *Genes Dev* 1996;10:985–996.
78. Mah AT, Yan KS, Kuo CJ. Wnt pathway regulation of intestinal stem cells. *J Physiol* 2016;594:4837–4847.
79. Davies PS, Powell AE, Swain JR, et al. Inflammation and proliferation act together to mediate intestinal cell fusion. *PLoS One* 2009;4: e6530.
80. Batlle E, Henderson JT, Beghtel H, et al. Beta-catenin and TCF mediate cell positioning in the intestinal epithelium by controlling the expression of EphB/ephrinB. *Cell* 2002;111:251–263.
81. Andreu P, Peignon G, Slomianny C, et al. A genetic study of the role of the Wnt/beta-catenin signalling in Paneth cell differentiation. *Dev Biol* 2008;324:288–296.
82. Watanabe N, Mashima H, Miura K, et al. Requirement of Ga-q/Ga-11 signaling in the preservation of mouse intestinal epithelial homeostasis. *Cell Mol Gastroenterol Hepatol* 2016;2:767–782.
83. Yin X, Farin HF, van Es JH, et al. Niche-independent high-purity cultures of Lgr5+ intestinal stem cells and their progeny. *Nat Methods* 2014;11:106–112.
84. Amin N, Vincan E. The Wnt signaling pathways and cell adhesion. *Front Biosci (Landmark Ed)* 2012;17:784–804.
85. Sun Y, Wang Y, Cao Q, et al. Expression and role of CD166 in the chronic kidney disease. *Iran J Pediatr* 2015; 25:e543.
86. Tachezy M, Zander H, Gebauer F, et al. Activated leukocyte cell adhesion molecule (CD166): its prognostic power for colorectal cancer patients. *J Surg Res* 2012; 177:e15–e20.

---

Received June 3, 2016. Accepted December 4, 2016.

**Correspondence**

Address correspondence to: Melissa H. Wong, PhD, Oregon Health & Science University, Department of Cell, Developmental and Cancer Biology, 3181 SW Sam Jackson Park Road, Mail Code L215, Portland, Oregon 97239. e-mail: wongme@ohsu.edu; fax: (503) 494-4253.

**Acknowledgments**

The authors are grateful for the assistance of the OHSU Flow Cytometry Shared Resource (Miranda Gilchrist, Philip Streeter, and Pam Canaday), for assistance from James Abe and John Swain, and for CLEM assistance from Chris Arthur (FEI, OHSU Multi-scale Microscopy Core) and Robert P. Smith (SUNY-ESF).

**Conflicts of interest**

The authors disclose no conflicts.

**Funding**

Supported by U01 DK085525, DK068326 (M.H.W.) and CA106195-09, Medical Research Foundation of Oregon ECI Award, OHSU Knight Cancer Institute Research Development Award, Knight Cancer Institute: P30 CA069533-17 (N.R.S.).